U.S. Department of Transportation
Federal Highway Administration

TN TDOT Department of Transportation

Utilization of Accelerated Pavement Tester (APT) for New Materials and Pavement Structure Research

Research Final Report from the University of Tennessee, Knoxville | Baoshan Huang ,Xi Jiang, and Pawel Polaczyk | May 30, 2022

Sponsored by Tennessee Department of Transportation Long Range Planning
Research Office & Federal Highway Administration

DISCLAIMER

This research was funded through the State Planning and Research (SPR) Program by the Tennessee Department of Transportation and the Federal Highway Administration under ***RES #2019-12: Research Project Title: Utilization of Accelerated Pavement Tester (APT) for New Materials and Pavement Structure Research.***

Technical Report Documentation Page

1. Report No. RES # 2019-12	2. Government Accession No.	3. Recipient's Catalog No.
4. Title and Subtitle *Utilization of Accelerated Pavement Tester (APT) for New Materials and Pavement Structure Research*		5. Report Date May 2022 6. Performing Organization Code
7. Author(s) Baoshan Huang, Xi Jiang, Pawel Polaczyk		8. Performing Organization Report No.
9. Performing Organization Name and Address Department of Civil and Environmental Engineering The University of Tennessee, Knoxville 851 Neyland Drive Knoxville, TN, 37996		10. Work Unit No. (TRAIS) 11. Contract or Grant No. RES # 2019-12
12. Sponsoring Agency Name and Address Tennessee Department of Transportation 505 Deaderick Street, Suite 900 Nashville, TN 37243		13. Type of Report and Period Covered Final report January 2019 - May 2022 14. Sponsoring Agency Code
15. Supplementary Notes Conducted in cooperation with the U.S. Department of Transportation, Federal Highway Administration.		

16. Abstract

Accelerated pavement test (APT) is defined as the controlled application of a prototype wheel loading at the appropriate load to the full-scale pavement structure, which is used to determine the structural responses and performance of the pavement in a short period. Inverted pavement is an unconventional type of flexible pavement structure. In this pavement structure, an unbound aggregate base (UAB) with a low initial modulus is layered between two stiffer layers, an asphalt concrete layer (AC) and a cement-treated base layer (CTB). This project presents two rounds of APT tests on full-scale inverted pavements. In the first-round APT, a comparison study on the rutting performance between the conventional and inverted pavement structures was presented. In addition, the inverted pavements with different thicknesses of UAB and CTB were studied. Significant permanent deflections were observed in all three pavement lanes after 100k passes of APT. Based on the measured deformation, the inverted pavement structure outperformed the conventional pavement in terms of the final surface deformation. And the inverted pavement with a thicker CTB layer had a better performance than the inverted pavement with a thicker UAB layer. Based on the overall pavement conditions, the inverted pavement can be regarded as an alternative to the conventional flexible pavement, and asphalt mixture layer thickness can be reduced during construction. In the second round of APT, the effect of geogrids in the inverted pavement was investigated. The polypropylene geogrids were installed in the full-scale inverted pavements and different locations of geogrids were discussed as well. After 150k passes of APT, the rutting performance was compared and studied. The results show that the geogrids could improve the rutting resistance of the inverted pavement, but the effect of geogrids depended on the location in the UAB layer. In this study, the geogrids placed at the upper 1/3 upper layer of UAB displayed the best rutting performance among the three pavement lanes due to its constraint for the aggregates. However, when the geogrids were installed at the 2/3 thickness of the UAB, the rutting performance of the inverted pavement structure became worse since its position experienced little tension and could not take effect. Therefore, the location of geogrids plays a vital role in improving the rutting resistance of the inverted pavement.

17. Key Words **ACCELERATED PAVEMENT TESTER (APT), INVERTED PAVEMENT, GEOGRIDS, PAVEMENT PERFORMANCE**	18. Distribution Statement No restriction. This document is available to the public from the sponsoring agency at the website http://www.tn.gov/.

19. Security Classif. (of this report) Unclassified	20. Security Classif. (of this page) Unclassified	21. No. of Pages 59	22. Price

Acknowledgement

We would like to thank the Tennessee Department of Transportation (TDOT) for funding this research project. We have continued to collaborate closely with regional engineers and local technicians. They have provided valuable support towards the fulfillment of the research objectives. Without their support, it would be impossible to finish this research project. We would also like to thank the administrative staff from the TDOT Research Office who have worked very closely with our research team and kept the whole project on the proposed schedule.

This project partially supported the publication of three peer-reviewed journal papers:

- Jiang, Xi, Hani Titi, Yuetan Ma, Pawel Polaczyk, Miaomiao Zhang, Jay Gabrielson, Yun Bai, and Baoshan Huang. "Evaluating the performance of inverted pavement structure using the accelerated pavement test (APT)." Construction and Building Materials 346 (2022): 128489.
- Jiang, Xi, Jay Gabrielson, Baoshan Huang, Yun Bai, Pawel Polaczyk, Miaomiao Zhang, Wei Hu, and Rui Xiao. "Evaluation of inverted pavement by structural condition indicators from falling weight deflectometer." Construction and Building Materials 319 (2022): 125991.
- Jiang, Xi, Miaomiao Zhang, Rui Xiao, Pawel Polaczyk, Yun Bai, and Baoshan Huang. "An investigation of structural responses of inverted pavements by numerical approaches considering nonlinear stress-dependent properties of unbound aggregate layer." Construction and Building Materials 303 (2021): 124505.

Executive Summary

The purpose of this study is to utilize the accelerated pavement tester at the University of Tennessee-Knoxville (UTK) campus to test and evaluate new pavement structure, and corresponding reinforcement method. Accelerated pavement test (APT) is defined as the controlled application of a prototype wheel loading at the appropriate load to the full-scale pavement structure, which is used to determine the structural responses and performance of the pavement in a short period [1]. Many state Departments of Transportation (DOTs) have adopted APT for their materials and pavement structure research, such as Louisiana DOTD, Florida DOT, and Virginia DOT. Under the sponsorship and leadership of the Tennessee Department of Transportation (TDOT), an APT has been successfully established at UTK and used in a research project entitled "Evaluation of Geosynthetics Reinforcement in Flexible Pavement Structures Using Accelerated Pavement Testing." TDOT participates in full-scale pavement testing at the National Center of Asphalt Technology Test Track and needs to take advantage of the APT as a convenient and versatile research approach for testing new pavement materials, innovative pavement structures, and pavement maintenance activities. With the ever-growing traffic volume and ever-tightening budget constraints, it is a great challenge for state highway agencies to keep the highway network operating smoothly. Many states have endeavored to explore new strategies that provide superior performance and are yet less costing, such as innovative pavement structure design, new pavement materials, cost-effective pavement maintenance, and rehabilitation methods. This research aimed to utilize the accelerated pavement testing device and pit at UTK to investigate the unconventional pavement structure-inverted pavement and its reinforcement methods.

The APT method is a highly efficient testing approach based on past studies. However, few studies have applied the APT method to investigate the structural responses of the inverted pavement. Therefore, the advantages of APT can be applied to test the inverted pavement structures. This project presents two rounds of APT tests on full-scale inverted pavements. In the first-round APT, a comparison study on the rutting performance between the conventional and inverted pavement structures was presented. In addition, the inverted pavements with different thicknesses of UAB and CTB were studied. Significant permanent deflections were observed in all three pavement lanes after 100k passes of APT. Based on the measured deformation, the inverted pavement structure outperformed the conventional pavement in terms of the final surface deformation. And the inverted pavement with a thicker CTB layer had a better performance than the inverted pavement with a thicker UAB layer. Based on the overall pavement conditions, the inverted pavement can be regarded as an alternative to the conventional flexible pavement, and asphalt mixture layer thickness can be reduced during construction. In the second round of APT, the effect of geogrids in the inverted pavement was investigated. The polypropylene geogrids were installed in the full-scale inverted pavements and different locations of geogrids were discussed as well. After 150k passes of APT, the rutting performance was compared and studied. The results show that the geogrids could improve the rutting resistance of the inverted pavement, but the effect of geogrids depended on the location in the UAB layer. In this study, the geogrids placed at the upper 1/3 layer of UAB displayed the best rutting performance among the three pavement lanes due to its constraint for the aggregates. However, when the geogrids were installed at the 2/3 thickness of the UAB, the

rutting performance of the inverted pavement structure became worse since its position experienced little tension and could not take effect. Therefore, the location of geogrids plays a vital role in improving the rutting resistance of the inverted pavement. Through the full-scale test coupled with APT, the detailed construction experience of the full-scale inverted pavement structure was provided, and the testing results can extend the understanding of the difference in structural responses between the inverted and conventional pavement structures. Therefore, this study is valuable for both the pavement industry and academia.

Key Findings

The key findings from this research project are summarized as follows:

- APT is a highly efficient testing method to investigate the structural responses of both the inverted and conventional pavement structures under a controlled loading and environmental conditions.
- Based on the overall rutting performance, the inverted pavement structure had a comparable or better performance compared with the conventional flexible pavement structure under the same loading and environmental conditions. Thus, the inverted pavement can be regarded as an alternative to the traditional flexible pavement.
- The inverted pavement structure differed from the conventional pavement structure in the accumulating permanent surface deformation with APT's passes. For the inverted pavement, three phases could be observed. When the loading passes reached a certain number (60k in this study), the UAB layer in the inverted pavement became much stiffer due to its stress-dependent property. Thus, the permanent deformation in the inverted pavement slowed down and the deformation curve became gentle. However, the rutting in the conventional pavement became more severe with the increasing loading passes because the stress-dependent property of UAB did not take effect in the conventional pavement due to its lack of a rigid CTB layer.
- The location of geogrids plays an important role in reinforcing aggregates in the UAB layer of the inverted pavement. In this study, geogrids placed at the upper 1/3 layer of UAB improved the rutting resistance of inverted pavement. However, geogrids installed at the 2/3 thickness of UAB resulted in worse rutting performance. Due to the stress-dependent property of UAB layer in the inverted pavement, the geogrids placed at the upper 1/3 layer could experience much higher tension and take effect to provide more constraints for the aggregates, contributing to the increase of its stiffness.

Key Recommendations

Based on the findings, the potential recommendations are summarized as follows:

- During the construction of inverted pavement structures, the compacted UAB layer should be left for one night before placing the asphalt concrete layer to lower its moisture.
- The aggregates for the UAB layer of inverted pavement should be treated carefully. The small particles of aggregates (≤0.025 mm) should be partially removed to strength the interlocking of aggregates during the loading.

- The geogrids can be used as reinforcement in the UAB layer and improve the rutting resistance of the inverted pavement structure but the location of geogrids is of great importance.

Table of Contents

List of Tables

List of Figures

List of Key Acronyms

Acronyms	*Definition*
APT	*Accelerated Pavement Test*
AC	*Asphalt Concrete*
UAB	*Unbound Aggregate Base*
CTB	*Cement Treated Base*
SG	*Subgrade*
FEM	*Finite Element Method*
ROD	*Rate of Deformation*
TBR	*Traffic Benefit Ratio*
RRR	*Rutting Reduction Ratio*

Chapter 1 Introduction

1.1 Problem Statement

Accelerated pavement tester is a pavement loading device with full-scale wheels that can be used to provide a quick, efficient, and effective tool for research in pavements. Many states Departments of Transportation (DOTs) have adopted APT for their materials and pavement structure research, such as Louisiana DOTD, Florida DOT, and Virginia DOT. Under the sponsorship and leadership of the Tennessee Department of Transportation (TDOT), an APT has been successfully established at UTK and used in a research project entitled "Evaluation of Geosynthetics Reinforcement in Flexible Pavement Structures Using Accelerated Pavement Testing." TDOT participates in full-scale pavement testing at the National Center of Asphalt Technology Test Track and needs to take advantage of the APT as a mid-level research approach for testing new pavement materials, innovative pavement structures, and pavement maintenance activities. With the ever-growing traffic volume and ever-tightening budget constraints, it is a great challenge for state highway agencies to keep the highway network operating smoothly. Many states have endeavored to explore new strategies that provide superior performance and are yet less costing, such as innovative pavement structure design, new pavement materials, cost-effective pavement maintenance, and rehabilitation methods. This research aimed to utilize the accelerated pavement testing device and pit at UTK to investigate the many options to improve pavement performance in Tennessee by using new pavement materials, pavement structure, and pavement maintenance and rehabilitation methods.

TDOT has long been trying to use the APT method to evaluate full-scale pavement structures including geosynthetic-reinforced pavement. In this study, this high-efficiency method was applied to evaluate the structural responses of inverted pavement.

1.2 Objectives

The main objective of this study is to apply the APT method to investigate the performance of inverted pavement structures and their reinforcement methods. To achieve this objective, the performance of a full-scale inverted pavement was investigated using the APT method, and a conventional flexible pavement under the same environmental and loading conditions was studied and compared in the first round of APT. In addition, the effect of geogrids on the structural performance of the inverted pavement was studied in the second round of APT in this project, which has never been conducted before. Through the full-scale test coupled with APT, the detailed construction experience of the full-scale inverted pavement structure was provided, and the testing results can also extend the understanding of the difference in structural responses between the inverted and conventional pavement structures. Therefore, this study is valuable for both the pavement industry and academia.

1.3 Report Organization

This report mainly consists of five chapters. In the first chapter, the background and motivation of this project were provided. In the second chapter, the literature review of the APT and inverted pavement was provided. The development of APT and inverted pavement was introduced in this section. The details of the two rounds of APT conducted at the University of Tennessee, Knoxville

were provided in the third chapter. In this section, the main testing methodologies such as APT, dynamic cone penetration (DCP) test and nuclear gauge test were introduced. In the fourth chapter, the whole construction processes of the inverted pavement were shown, and the testing details and results from the two rounds of the APT were discussed. The performance of the inverted pavement was investigated by analyzing the road surface deformation. The mechanism of the geogrid-reinforcement in the inverted pavement was also revealed after the loading process by APT was finished on the geogrid-reinforced inverted pavement. In the last chapter, main conclusions of this project were drawn based on all the tests results and discussions.

Chapter 2 Literature Review

2.1 Accelerated Pavement Test (APT)

Accelerated pavement test (APT) is defined as the controlled application of a prototype wheel loading at the appropriate load to the full-scale pavement structure, which is used to determine the structural responses and performance of the pavement in a short period [1]. The APT facilities used on public roads have been developed in the United States since 1924 [1,2]. Compared with traditional field investigations, the full-scale test using the APT facility has many advantages, such as controlled loading and environmental conditions. In addition, APT has the capacity to perform the full-scale test in a shorter testing time. Thus, several previous studies have applied APT facilities to pavement-related experimental work. Ling et al. [3] investigated the rutting condition of airfield composite pavement by using APT. In this study, the APT method was utilized to control the temperature variations and load level, which extended the understanding of structural responses of airfield pavement. Ingrassia et al. [4] investigated the effect of geocomposite reinforcement on thin asphalt pavements with the APT facility. The permanent deflection after wheel passes of APT was compared. In this study, the APT approach contributed to the cost-effective and long-lasting pavement rehabilitation method. Fladvad and Erlingsson [5] studied the permanent deformation characterization of large-size unbound materials using a heavy vehicle simulator (HVS)-based APT under different moisture conditions. In this study, the groundwater table was changed to investigate the influence of gradation on moisture dependency. Han et al. [6] used the APT facility to evaluate the reinforcement effect of geogrids in conventional flexible pavements; 100,000 passes of 1.40 megapascal (MPa) tire pressure were applied to each testing lane and the corresponding accumulating rutting were compared between each lane.

2.2 Inverted Pavement

Inverted pavement is an unconventional type of flexible pavement, first constructed in South Africa in the 1950s. The structure of inverted pavement is different from the traditional flexible pavement because a thinner asphalt concrete (AC) layer and a stiffer CTB are placed in the inverted pavement, as shown in Figure 2-1. The UAB with a small initial modulus is placed between the two stiffer layers of AC and CTB. The stiffness of each layer decreases with the pavement depth in the conventional pavement. Thus, the inverted pavement structure has been a hot topic and attracted more and more interest from industry and academia.

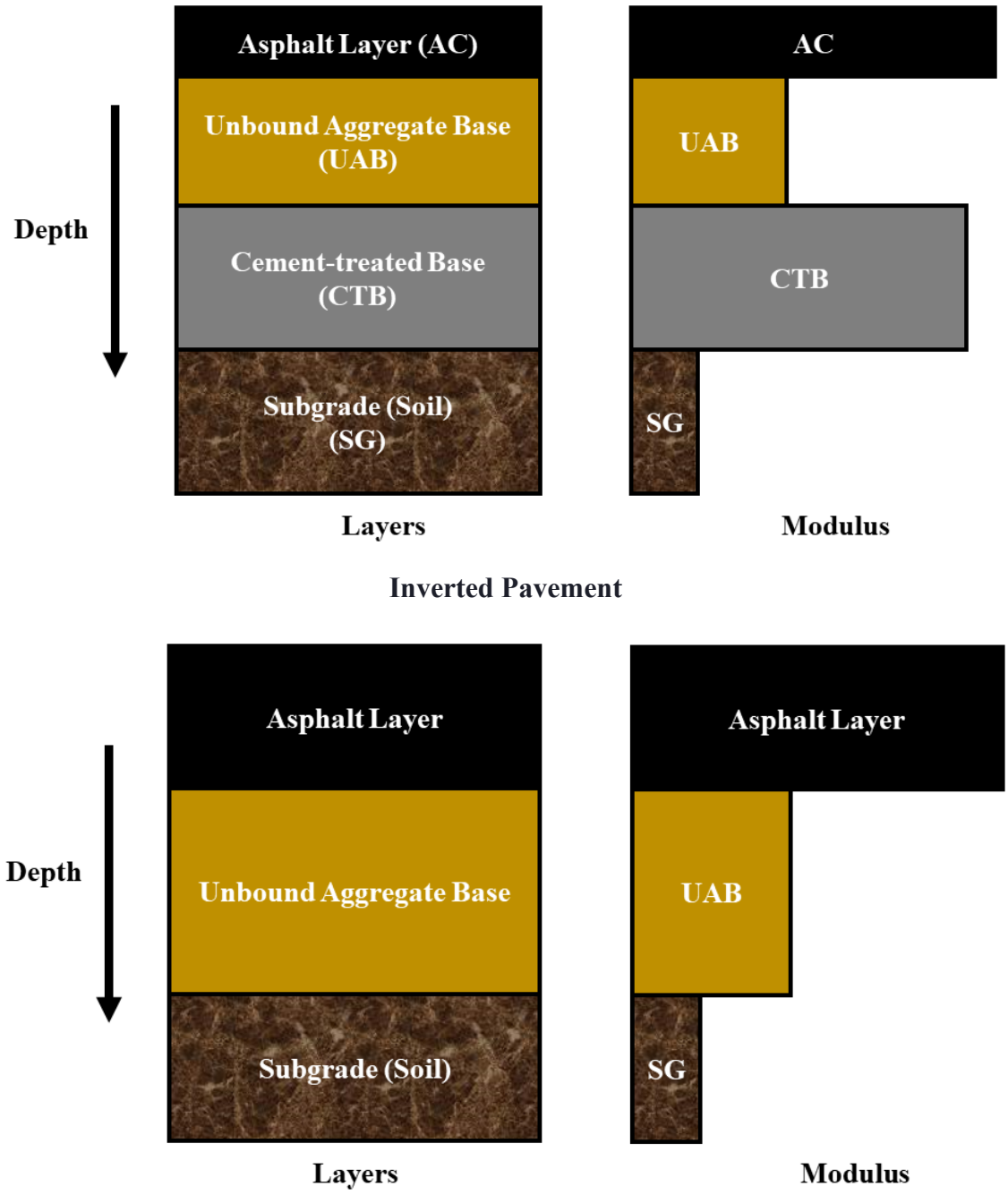

Figure 2-1. Comparison of inverted pavement and conventional pavement structures

Many scholars and engineers have conducted inverted pavement related laboratory experiments and field investigations in recent years. Lewis et al. [7] introduced the construction and performance of Morgan County and LaGrange Bypass inverted pavement projects in Georgia, USA. In the field investigation, the performance, such as rutting and cracking conditions, were compared between the inverted and conventional sections. The comparison study showed that

the inverted pavement sections were good in performance and cost-effective during the construction process. Cortes and Santamarina [8] gave a macro-scale complementary analysis and preliminary numerical studies on the LaGrange inverted pavement. The nonlinear stiffness-stress-dependent property of UAB in the inverted pavement was emphasized in this research, which helped to understand the inverted structures. In the numerical studies, more attention was placed upon the UAB layer because the stress-dependent stiffness of the granular materials had a significant influence on the inverted pavement structure. This study reported and illustrated the characteristics of the inverted pavement through numerical simulation. The finite element method (FEM) simulation by Papadopoulos and Santamarina [9] showed that the AC in the inverted structure developed lower tensile strains and resulted in longer fatigue life, proving that the inverted pavement was an economical alternative to the conventional flexible pavement due to its less asphalt mixture requirement.

Biswal et al. [10] investigated the structural response of the inverted pavement considering the isotropic and anisotropic properties of UAB. Jiang et al. [11] made a comparative study between the inverted and conventional pavements using the nonlinear simulation approach in the ABAQUS software. The results showed that the nonlinear stress-dependent property of UAB played an important role in the inverted pavement, but the little effect could be found in the conventional structure under the same loading and boundary conditions. In addition, the inverted structure experienced less tensile stress at the bottom of AC and less surface deflection was found compared with the conventional pavement lane. In Jiang's recent research, the deflection basin parameters (DBPs) from the falling weight deflectometer (FWD) were used to evaluate the performance of the inverted pavement. The modulus of each layer in the inverted pavement was adjusted to investigate the influence of individual layer on the overall performance of inverted pavement. The analysis results were consistent with the testing data obtained from a full-scale inverted pavement project in Tennessee, USA [12]. The recent literature mainly focused on numerical studies, and limited studies have been made on field investigations and macro-scale studies.

Chapter 3 Methodology

3.1 Accelerated Pavement Test (APT)

A full-scale accelerated pavement testing system simulated the wheel loads on the test sections. The equipment had the dimension of 8.5 m length × 2.5 m width × 2.5 m height (see Figure 3-1). Figure 3-1 (a) and (b) show the external and internal frameworks of the testing machine, respectively. A dual-wheel loading system with the bi-direction moving mode was applied in this study. The size of each loading wheel was 110 cm in diameter and 25 cm in width. The length of the wheel motion trajectory on the testing pavement was 5.5 m based on the measured tire marks. To ensure the smooth operation of the APT equipment, the running speed of the dual-wheel system was set at 3.6s/pass (1,000 passes/hour) and a load of 80 kN, which was twice the standard axle load, was applied. The contact pressure between the wheel and pavement surface was 1.4 MPa in this study. In addition, the temperature of the APT indoor lab was set at 20 ℃ to avoid the influence of temperature on the road surface deformation.

(a) (b)

Figure 3-1. The accelerated pavement testing (APT) facility

3.2 Construction Quality Control

Dynamic cone penetration (DCP) test was also used in this study to evaluate the strength of underlying subgrade (SG) and UAB by measuring the penetration of the device into the soil after each hammer below. In addition, the penetration results can be used to predict the modulus of the individual layer in pavement sections based on standard ASTM D6951, as shown in Figure 3-2. The penetration rate of DCP is related to the California Bearing Ratio (CBR), which can predict the strength of the SG and UAB layers based on the tabulated correlation of CBR versus DCP index. CBR profiles are related to the penetration rate of the DCP in mm/blow according to ASTM 6951.

(a)

(b)

Figure 3-2. (a) Process of DCP test; (b) Process of nuclear gauge test

Chapter 4 Results and Discussion

4.1 Experimental Program (1st Round)

4.1.1 Construction of test sections

The testing sections were located at UTK. As shown in Figure 4-1 (a & b), the thicknesses and layout of the layers are presented. The inverted pavement lanes I and II are constructed at the right and left sides to keep the same boundary condition. The conventional pavement section was paved at the middle lane as the benchmark for comparison. In addition, the wooden slabs were inserted at the boundaries of middle lane to separate the lanes and keep the same boundary conditions. The thickness of the AC layer, UAB layer, and subgrade is 127 mm (5 inches), 254 mm (10 inches) and 534 mm (21 inches), respectively. The thickness of the AC layer is 63.5 mm (2.5 inches) in the two inverted pavement lanes and 127 mm (5 inches) in the conventional pavement lane.

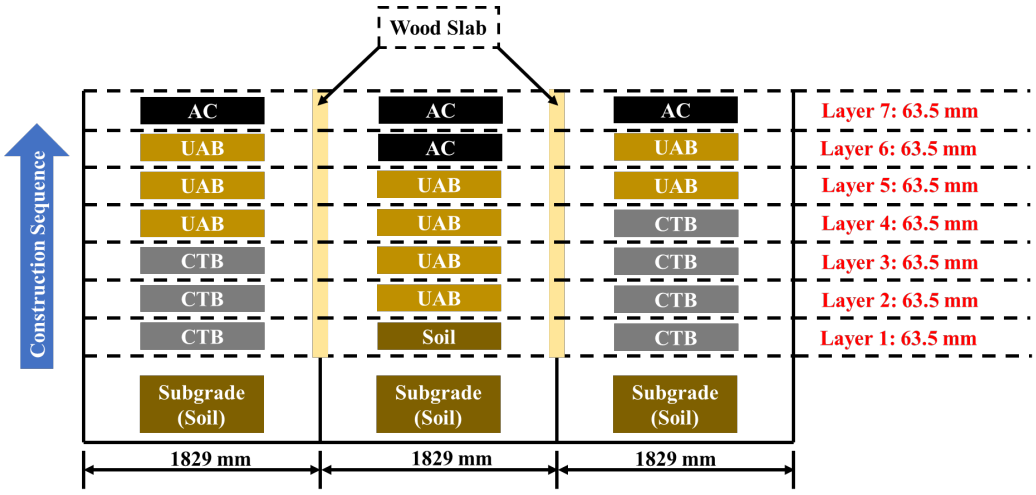

(a)

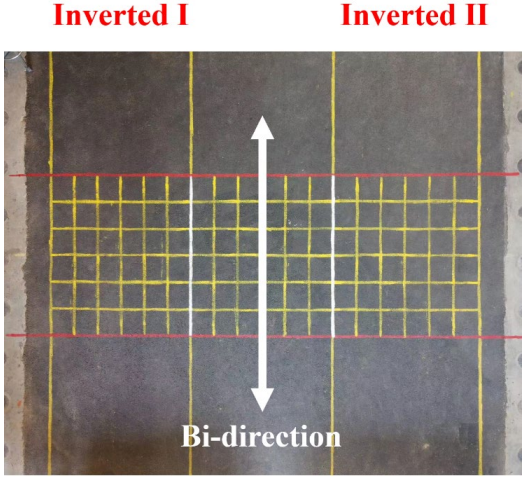

(b)

Figure 4-1. (a) The schematic design of testing pavement; (b) Testing pavement lanes for APT

Figure 4-2 shows the construction processes of the testing pavement. The filling and compaction processes of subgrade soil for inverted and conventional pavement sections are shown in Figure 4-2 (a & b). The wooden slabs were set up to separate pavement lanes in the pit, as shown in Figure 4-2 (c). During the construction of CTB, 6 % (by weight) of ordinary Portland cement was added to the soil, and a tiller mixed them. During the one-week curing, the moisture was kept by spraying water on the CTB and then a plastic sheet was used to cover the pit. After 7-day curing of CTB, UAB was placed above the CTB. After compaction of UAB for each pavement lane, the AC was paved as the surface.

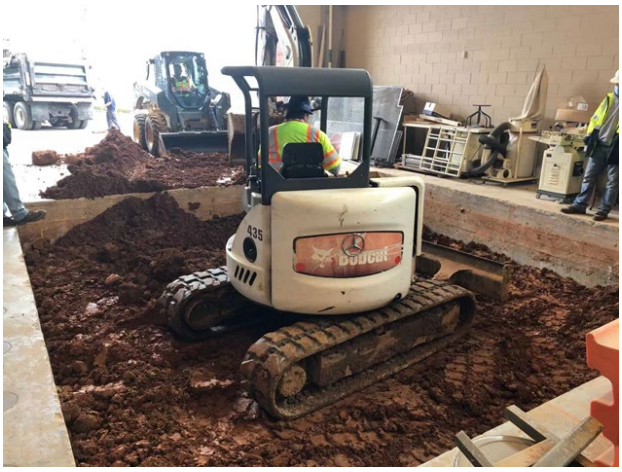

(a)

(b)

(c)

(d)

(e)

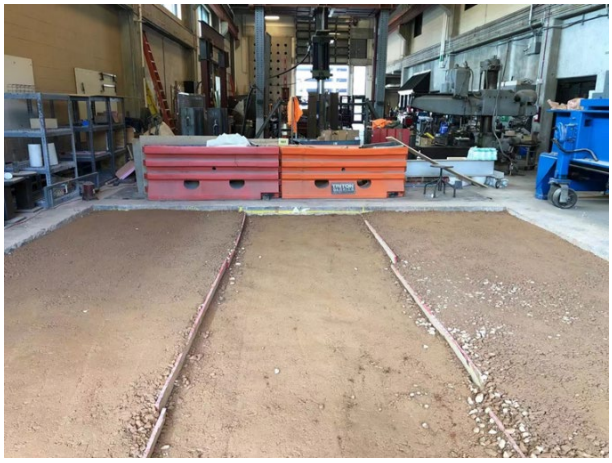

(f)

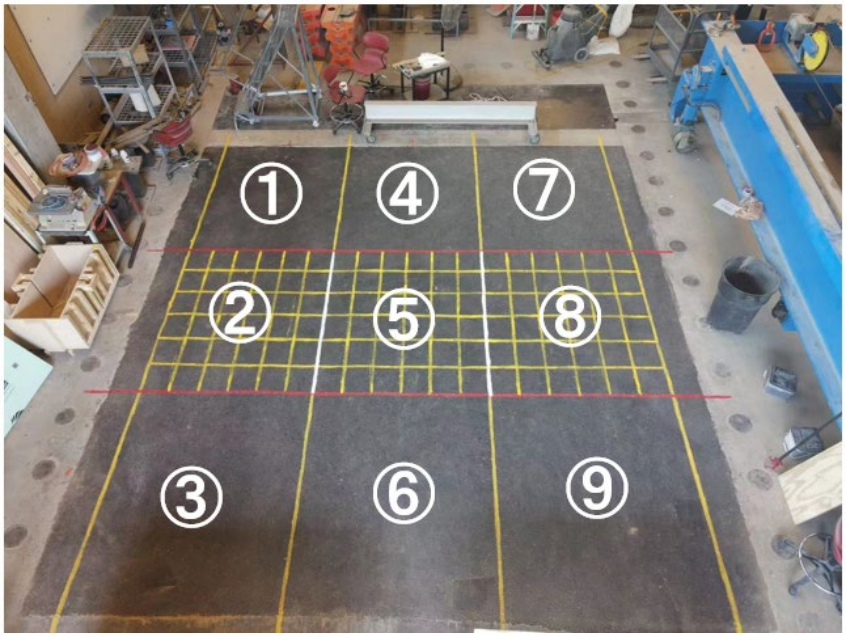

(g)

Figure 4-2**.** (a-f) Construction processes of the testing pavement; (g) Top view of the testing pavement

4.1.2 Materials selection and properties

4.1.2.1 Subgrade soil

In this full-scale test of inverted and conventional pavement sections, the subgrade soil was collected from Knoxville, TN, USA. The optimum moisture content (OMC) is 9.6%, and the maximum dry density (MDD) is 19.6 kN/m^3 (125.9 pcf) tested by the standard compaction method according to Standard AASHTO T 99-15. According to the laboratory tests, the subgrade soil is categorized as clayey silt (CL-ML) according to the standard ASTM D2487. Figure 4-3 shows the gradation of the subgrade soil and unbound aggregates for UAB.

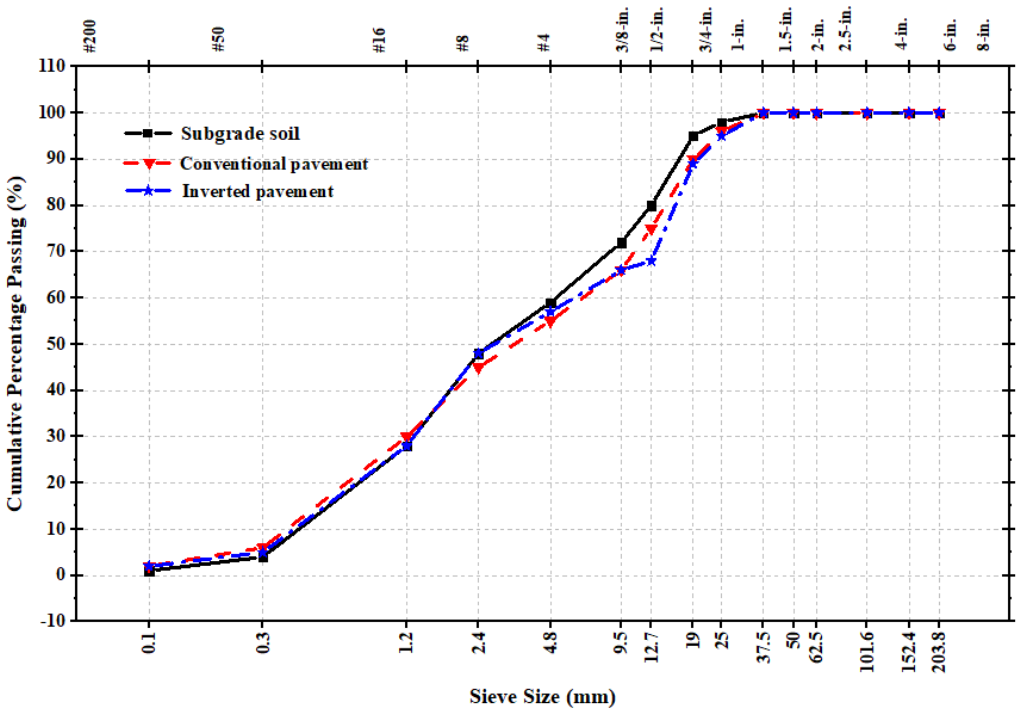

Figure 4-3. Gradation of the subgrade soil and unbound aggregates for UAB

4.1.2.2 Unbound aggregate materials

The unbound aggregate materials used for UAB are from Vulcan Quarry, Knoxville, TN, USA. The particle size distribution of unbound aggregate materials is also shown in Figure 4-3, and it can be classified into Grade D aggregate [13]. The OMC and MDD obtained from laboratory test is 6.9% and 22.1 kN/m^3 (140.5 pcf), respectively. There is a difference in the aggregate between the conventional and inverted sections. Less finer aggregates were used for the inverted section, and the aggregates on the 1/2 inch-sieve were removed in this study. Based on the gradation of aggregates used in UAB, the difference of the aggregates between the inverted and conventional pavements is little and can be neglected.

4.1.2.3 Cement-treated materials

In this study, the method to build CTB followed the approach by the Louisiana DOT to mix subgrade soil with 6% (by weight) ordinary Portland cement [14,15]. The compression test was conducted according to the standard ASTM D 1633 and the compressive strength of cement-treated materials for seven days in the laboratory is 2.2 MPa (321 psi) and the test specimen moisture content is 7.5%.

4.1.2.4 Asphalt concrete materials

The asphalt mix used in this study is 411-D with the asphalt binder PG 64-22 from TDOT with a density of 1040 kg/m^3 and the bulk density of the aggregate is 2510 kg/m^3. The AC (ACS-HM) in this study has a theoretical density of 2470 kg/m^3 and optimum asphalt content of 5.70%.

4.1.3 Layers' Properties

To control the construction quality of the pavement, the nuclear gauge test, as shown in Figure 3-2 (b), was conducted on each layer of the testing pavement to verify the compaction. A total of nine testing points were chosen, as shown in Figure 4-2 (g), to ensure the compaction quality of the whole testing pavement. The compaction and moisture content of SG and UAB are presented in Table 4-1. To achieve suitable compaction, the subgrade layer was compacted by three layer-iterative procedures. Based on the data in Table 4-1, the SG and UAB were in good compaction.

Table 4-1

Moisture content and compaction degree of SG and UAB

Section	***Compaction (%)***		***Moisture content (%)***	
	SG	*UAB*	*SG*	*UAB*
1	94.6	96.7	14.9	5.3
2	95.7	97.5	14.3	5.2
3	92.4	98.1	15.1	5.4
4	93.5	97.7	14.2	5.6
5	94.3	96.4	13.8	5.6
6	95.6	97.1	13.6	5.8
7	94.7	95.3	13.4	5.5
8	92.9	98.1	14.5	5.7
9	93.8	97.5	14.3	5.4
Average Value	94.2	97.1	14.2	5.7
Standard Deviation	0.53	0.18	1.06	0.85

Figure 4-4 presents the predicted CBR of the SG, UAB, and CTB layers based on the penetration depth from the DCP test and standard ASTM D6591. The SG has the minimum strength with an average CBR of 15%, and CTB has the largest strength with an average CBR of 86%. The achieved CBR is larger than the laboratory value due to the higher compaction levels from the heavy roller compared with the standard Proctor test [16]. Based on the DCP data, it is found that the strength of UAB is a little larger than SG, reflecting the initial strength of UAB without loading is small.

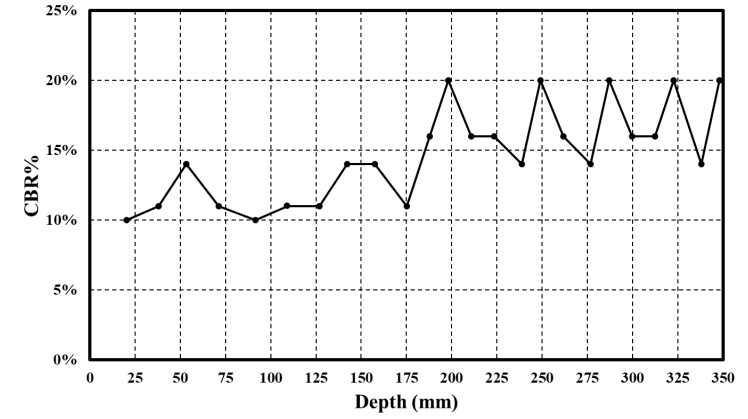

(a)

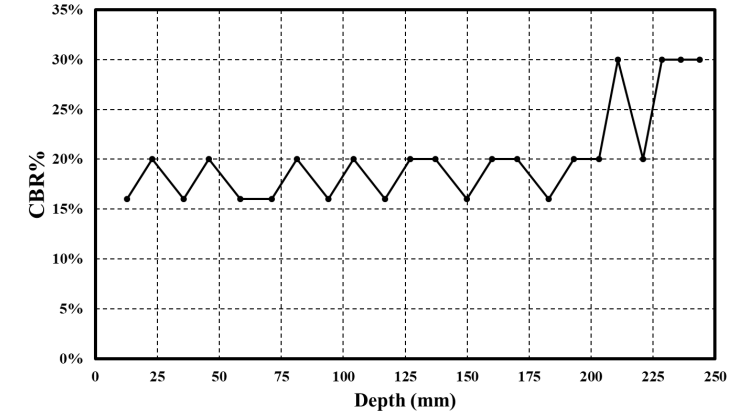

(b)

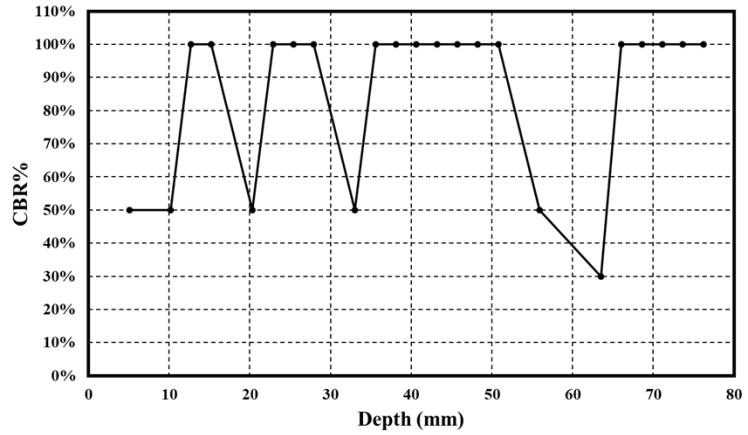

(c)

Figure 4-4. Relationship between penetration depth and CBR: (a) SG; (b) UAB; (c) CTB

For the construction of the AC layer, the plant asphalt mix was delivered by the dump trucks 30 mins before the surface construction. The target air voids percent (Va %) was set at 8%. To ensure the consistency of compaction, a hand-held compactor was used to compact the edge areas of the testing pavement. For the thickness validation, the individual thickness for each pavement lane was confirmed by digging transverse trenches after completing all APT tests.

4.1.4 Measurement of permanent surface deformation

A digital measuring instrument was used to measure the rutting depth and deformation of the testing pavement lanes with the loading passes, as shown in Figure 4-5 (a). The measurement results were based on the reference outside the testing pit. A total of 100,000 repetitious loading passes were applied to the testing pavements. The permanent surface deformation in this study was defined as the accumulating elevation difference of the measuring points on the pavement surface. In this study, the elevation difference at fixed loading passes of 2k, 4k, 6k,8k 10k, 15k, 20k, 25k, 30k, 40k, 50k, 60k, 70k, 80k, 90k, and 100k were recorded to investigate the change in the pavement profile. As shown in Figure 4-5 (b), each testing pavement lane was painted with lines for deformation measurement. And more measuring points were added near the wheel loading area to exclude the influence of boundary effects, as shown in Figure 4-5 (c). Each testing pavement lane was divided into 13 rows for the transverse profile and 13 columns for the longitudinal profile. In addition, the corresponding points were marked with numbers for easier and more convenient calculation and statistics.

(a)

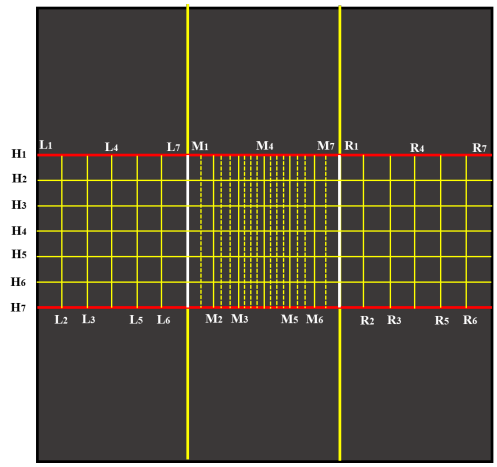

(b)

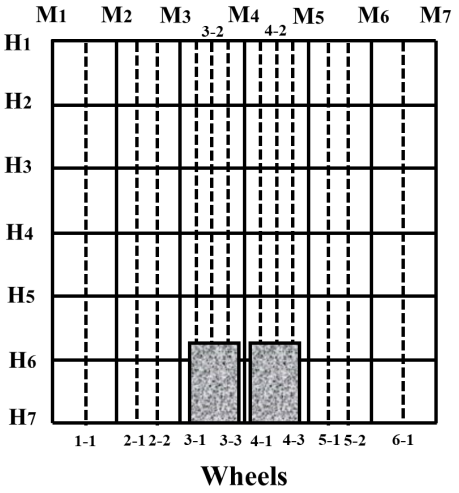

(c)

Figure 4-5. (a) Measurement of deformation of testing pavement; (b) Measuring point on testing pavements; (c) Detailed measuring points on the middle lane

4.2 Performance evaluation (1st round)

4.2.1 Surface deformation with passing times

After different loading passes by the APT facility, surface deformation was detected and measured in each pavement lane. Figure 4-6 shows each testing pavement lane's final surface deformation contours along the longitudinal wheel path after finishing the wheel-loading process. Based on the presented data, it can be found that the influencing area for each lane was within the central 100 cm. The area of the outer 30 cm at two sides of each lane was not affected by the moving wheels. Therefore, the boundary effect of the two adjacent lanes could be neglected in this test, which provided comparable deformation results for this study. The black points in Figure 4-6 represent the measuring points to detect the pavement deformation. Based on the deformation data in Figure 4-6, the maximum deformation area is located between 600 mm and 1200 mm from the origin point in all three pavement lanes because this area is along the wheel path. The largest deformation of 26.7 mm was found in the conventional pavement (middle) lane; the largest surface deformation of inverted pavement I was 24.4 mm, which was worse than 19.9 mm of deformation in inverted pavement II. Furthermore, the general condition of surface deformation in the conventional lane is more severe than the inverted structure. Inverted pavement II with a thicker CTB had better performance than inverted lane I with a thicker UAB.

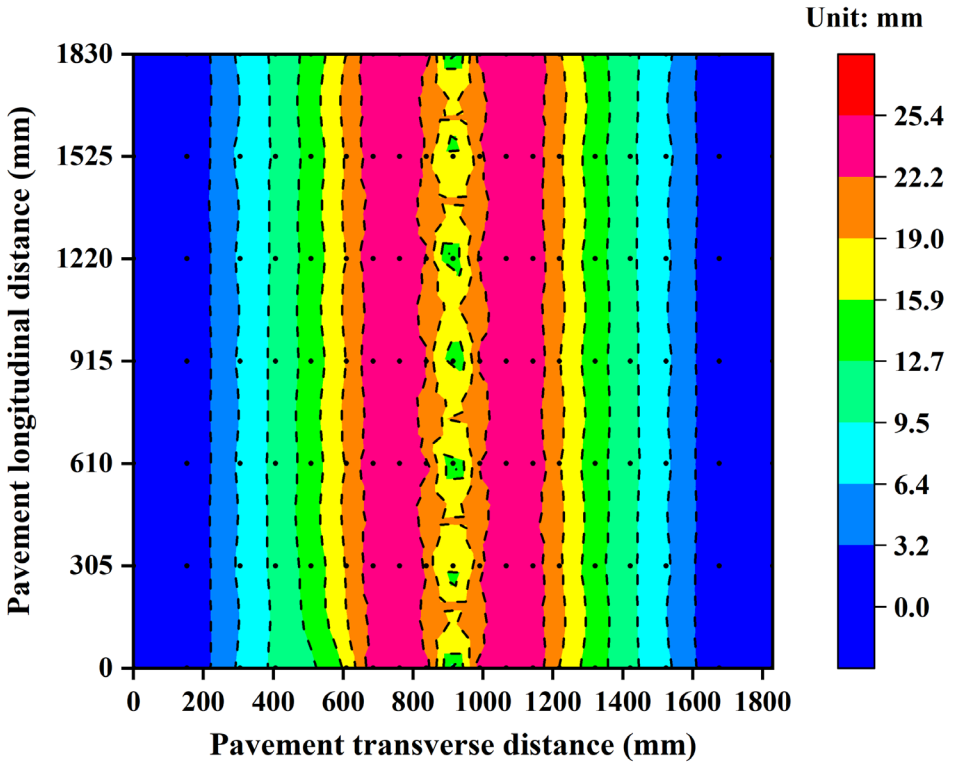

(a)

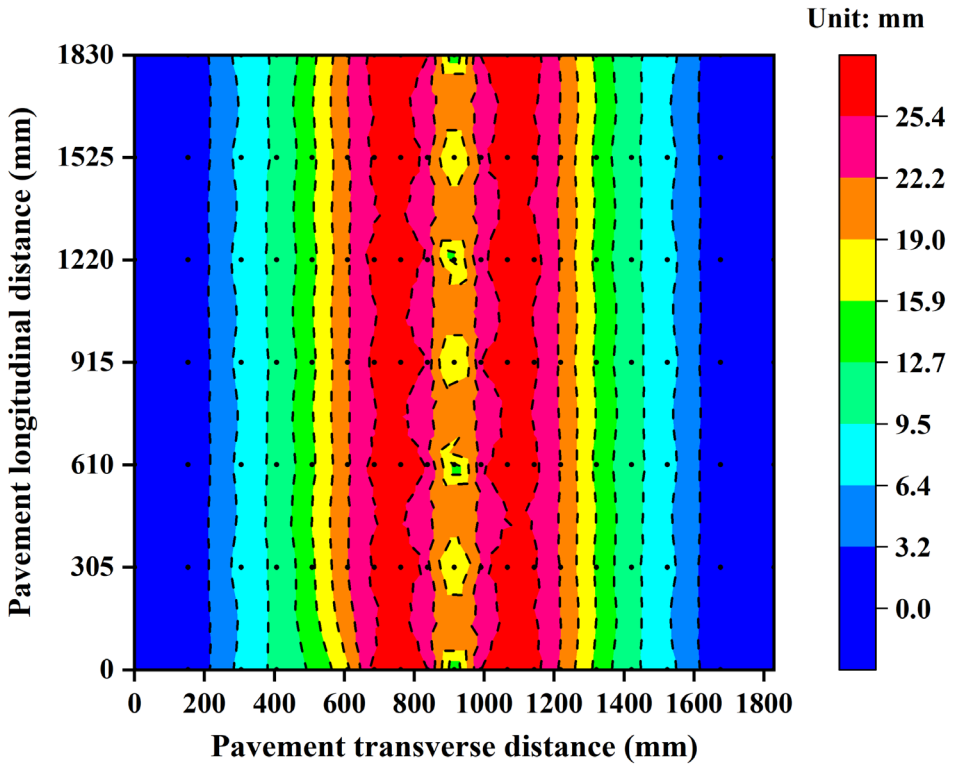

(b)

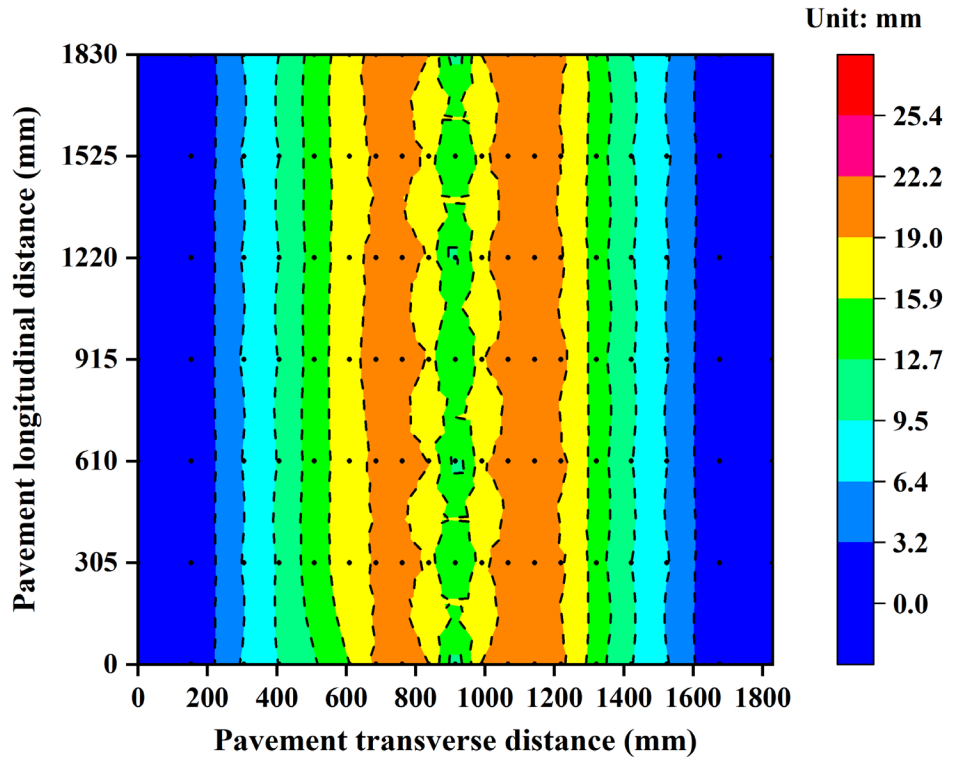

(c)

Figure 4-6. Final surface deformation contours of each testing pavement lane (a) Inverted pavement I; (b) Conventional pavement; (c) Inverted pavement II

Figure 4-7 exhibits the surface profiles in transverse direction due to bi-directional accelerated pavement loading passes. In this study, after completing the measurement for each lane, all the data were calibrated based on the initial pavement profile. Thus, the initial profile elevation at the beginning is 0 mm. The rutting failure criterion was set as 25.4 mm (1 inch), considering the APT facility's experimental time and stroke limitation. The rutting failure criterion of 25.4 mm was chosen based on the past experimental experience [17]. Based on Figure 4-7, the non-uniform W-shaped deformation with double peaks was observed in the dual-wheel rutting profiles, and an uplift was found between the dual wheels for three lanes. As for the final deformation, the conventional lane and inverted I had a comparative performance on the maximum profile elevation, and both exceeded the failure criterion, but the inverted pavement I had a smaller failure area than the conventional lane. For the two inverted pavement lanes, the profile elevation of inverted pavement II was within the failure criterion, indicating its better performance than the other two lanes.

There is an interesting phenomenon to be noticed in Figure 4-7. The shape of curves of inverted pavement has a wider waist compared with the conventional structures, which indicates that a larger area was affected due to the surface loading in the inverted pavement structure. The affected area of inverted lane II is also wider than that of inverted lane I, which might be due to the thicker CTB layer. The larger affected area but lower permanent deformation in the inverted structure might be due to the function of the CTB layer. The thicker CTB coupled with UAB re-distributed the stress in the pavement and resulted in a larger affected area, which has been validated in the numerical simulation by Jiang et al. [11].

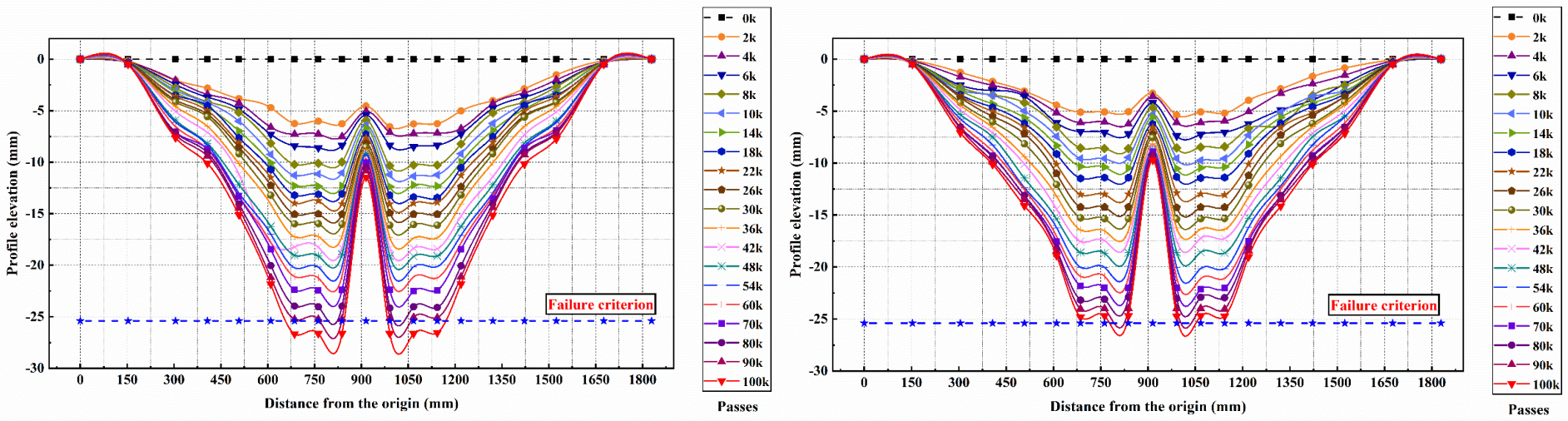

(a)

(b)

(c)

Figure 4-7. Pavement profile of (a) Conventional lane, (b) Inverted pavement I, (c) Inverted pavement II with loading passes

Figure 4-8 shows the accumulating permanent deformation concentrated on the wheel-loading areas; the average value of measuring points $M_{3\text{-}1}$, $M_{3\text{-}2}$, $M_{3\text{-}3}$, $M_{4\text{-}1}$, $M_{4\text{-}2}$ and $M_{4\text{-}3}$ were plotted. Based on the data curve, the entire deformation process of pavements could be divided into three phases. In phase one, all three pavement lanes experienced an accelerating increase in surface deformation. This change was mainly due to the rapid densification from the loading wheel. The conventional pavement contains a thicker UAB layer than the inverted structures, thus, a steeper curve could be observed for the conventional lane. Phase two with a stable development and gentle curve occurred next. In this phase, the permanent surface deformation increased slowly in three lanes, and the permanent deformation came to the same value when the number of passes reached 60k. The deformation of inverted lane I contributed 32.4% to the final deformation. The reason why the deformation of inverted lane I increased a lot during this phase is the relatively thin AC layer and more compaction in the UAB layer. After 60k passes, the deformation in three lanes gradually slowed down in the inverted pavement lanes, but the conventional lane's deformation rate remained constant. Based on the condition in phase three, the fatigue of conventional pavement further deepened but the inverted pavement lanes presented a better performance. The deformation of SG and UAB led to the larger profile elevation in the conventional pavement structure.

On the contrary, the stiffness of the UAB layer in the inverted pavement structure increased significantly with the loading passes. Therefore, the stiffer UAB could provide a cushion for the thin AC layer. The reflective cracks generated from the lower part of the pavement could be prevented by the UAB, which resulted in the longer service life of the pavement and lower rutting. Thus, the inverted pavement I had a smaller permanent deformation than that of the conventional lane when 100k loading passes were reached. Based on the overall performance, the inverted pavement II had the best condition after 100k passes of loading. The conventional pavement had a comparative performance with the inverted pavement I based on the value of final deformation.

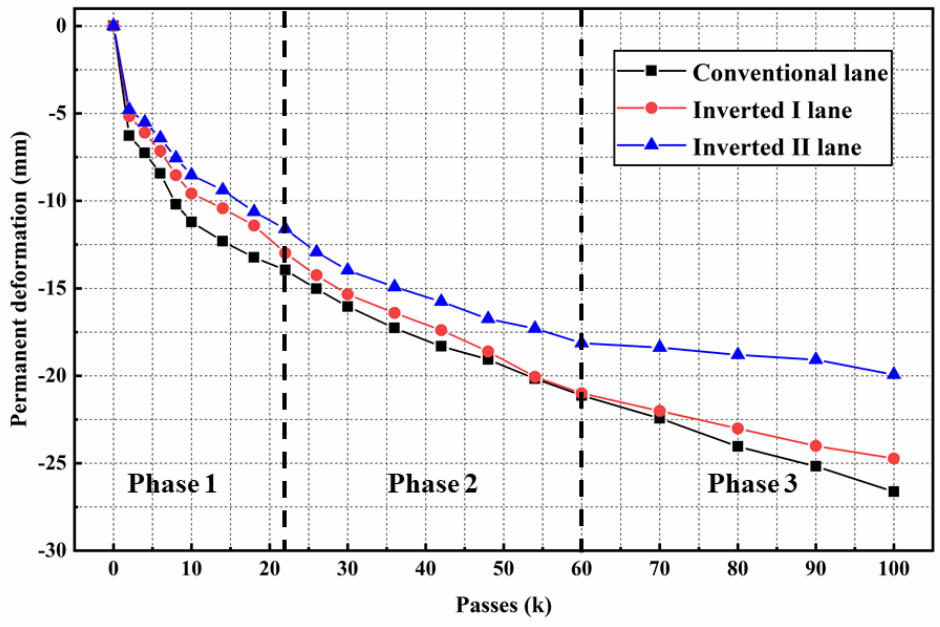

Figure 4-8. Accumulating permanent surface deformation for three lanes

4.2.2. Pavement trenches investigation

To investigate the deformation in individual pavement layers in detail, the testing pavement was trenched at the middle section after finishing the APT tests, as shown in Figure 4-9. The permanent deformation could be measured easily at the pavement section, which could also be used to validate the measurement on the surface. According to Han et al. [6], the total permanent surface deformation was calculated by adding the deformations of surface, base, and subgrade. In this study, the deformations below the CTB layer were hard to measure from the cross-section because the CTB layer had much higher stiffness, and little deformation could be found. Based on the cross-sections, it can be easily observed that the AC surface in conventional and inverted I lanes had larger deformation, and the top of UAB in these two lanes also had larger deformations. The results from the pavement trenches verified the measurements discussed in earlier sections of this study. The less deformation at the top of the UAB layer in the inverted pavement structures indicated that less tension occurred at the surface of the AC layer, which showed that inverted structures contributed to preventing the generation of cracks at the bottom of AC layer. Another reason for this phenomenon was because the UAB layer in the inverted pavement was stiffer than that in the conventional pavement. In addition, the thicker CTB layer in the inverted pavement II had a better performance than inverted pavement I, which meant thicker CTB coupled with UAB layer contributed to the rutting performance and mitigated the potential reflective cracks generated from the CTB in the inverted pavement. Therefore, the trenches results showed that the inverted pavement structures outperformed the conventional flexible pavement structure or had a comparative performance compared with the traditional pavement structures.

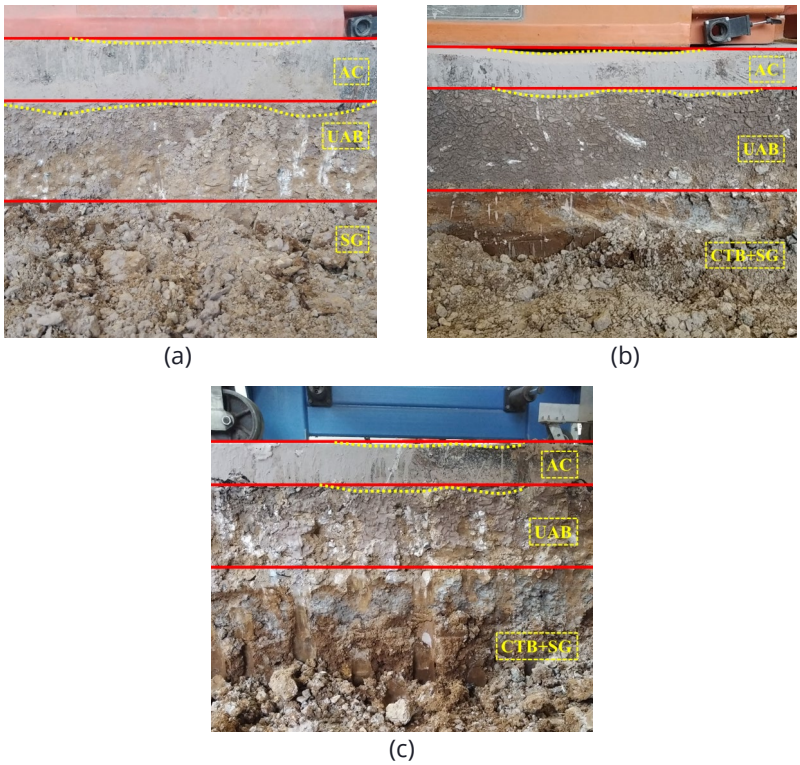

Figure 4-9. Trench sections at the middle of (a) conventional pavement, (b) inverted pavement I, (c) inverted pavement II

4.3 Experimental program (2nd round)

4.3.1 Construction of test sections

The testing sections in the 2nd round of APT were also located at UTK. As shown in Figure 4-10, the thickness and layout of the pavement layers are presented. The whole testing pit was divided into three road lanes with the same layers' structures. The thickness of the AC layer, UAB layer, and CTB layer is 6.4 cm (2.5 in.), 15.3 cm (6 in.), and 22.8 cm (9 in.), respectively. s

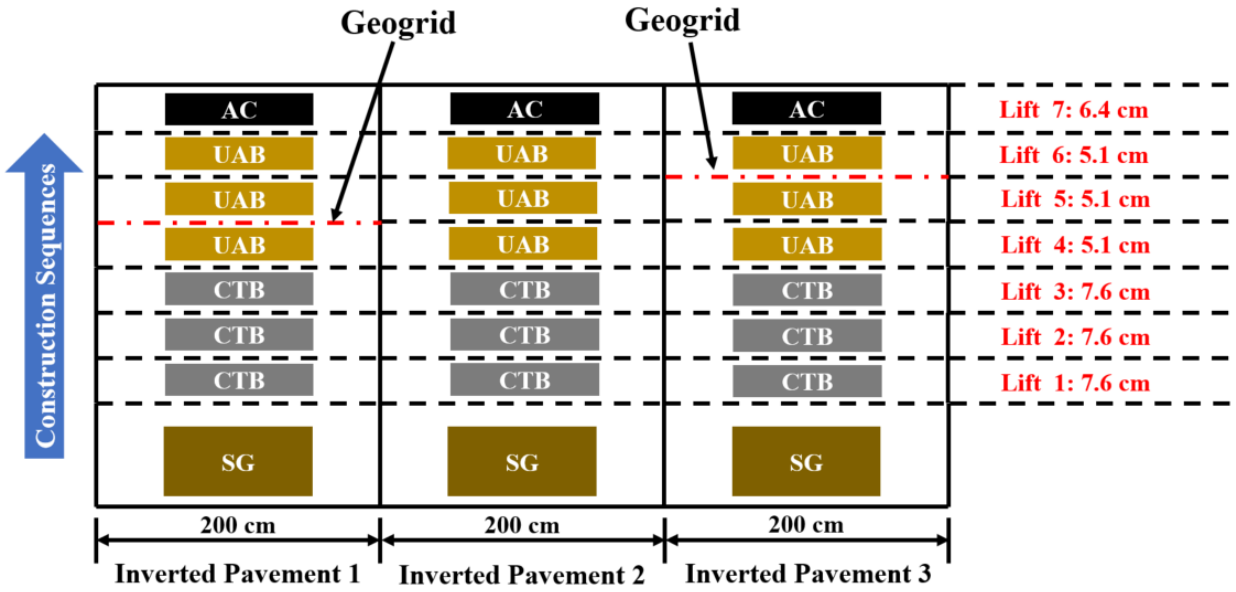

Figure 4-10. Schematic design of testing inverted pavement

The whole construction processes of the 2nd round of APT are displayed in Figure 4-11. The construction team removed the old testing pavement materials and refill subgrade soil to meet the requirement of thicknesses, as shown in Figure 4-11 (a). In order to have better compaction of the pavement layer, the portable compactor was used to compact the boundaries of the testing pavement, as shown in Figure 4-11 (b). In Figure 4-11 (c), 4% (by weight) of the ordinary Portland cement (Type Ⅰ) was mixed with the aggregates by a portable tiller to build the CTB layer. During the mix of CTB layer, the tap water was sprayed on the CTB layer to help develop its early strength. After the compaction of the CTB layer, it was cured for seven days. During the curing time, tap water was sprayed on the surface of CTB layer twice a day to keep the moisture, contributing to the late strength of cementitious mixtures in the CTB layer. In addition, the pit was sealed by a plastic membrane. The CTB layer after 7-day curing is shown in Figure 4-11 (d). The UAB layer was placed on top of CTB, as shown in Figure 4-11 (g). During the placement of the UAB layer, the geogrids were installed within the unbound aggregates, as shown in Figure 4-11 (e). The AC layer was placed at the pavement surface, as shown in Figure 4-11 (h). The laser elevation correction system was applied during the construction to guarantee the thickness of each layer, as shown in Figure 4-11 (f).

(a)

(b)

(c)

(d)

(e)

(f)

(g) (h)

Figure 4-11. Construction processes of the testing inverted pavements

4.3.2 Materials selection and properties

4.3.2.1 Subgrade soil

The subgrade soil for the 2nd round of APT was also collected from Knoxville, TN, USA. The particle distribution of the subgrade soil is presented in Figure 4-12 (black line). Based on the standard compaction method according to Standard AASHTO T 99-15, the optimum moisture content (OMC) is 14.7%, and the maximum dry density (MDD) is 1792 kg/m^3. Based on the laboratory tests, the subgrade soil is categorized as clayey silt (CL-ML) according to the standard ASTM D2487, and it can be classified as 7-6 soil in the AASHTO classification system.

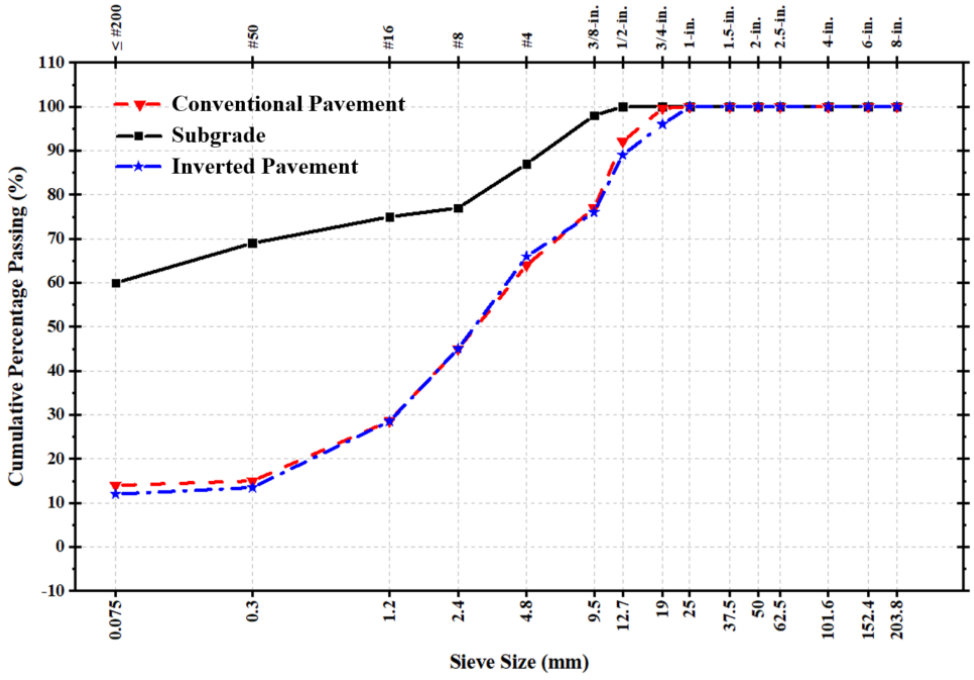

Figure 4-12. Particle distribution of the subgrade soil and unbound aggregates for UAB

4.3.2.2 Aggregates (UAB)

The unbound aggregates used for the UAB layer are also provided by the Vulcan Materials Company in Knoxville, TN, USA. The gradation of the aggregates for the inverted pavement is

shown in Figure 4-12 (blue line). Based on the particle distribution of the aggregates in the UAB layer, it can be found that fewer small particles (≤0.075 mm) were used in the inverted pavement compared with the typical TDOT Grade aggregates [13]. Less small particles in the UAB layer contribute to the interlocking of the aggregates, resulting in a larger modulus of the UAB layer after the repetitious loadings. According to the AASHTO 180-15 standard, the OMC and MDD obtained from laboratory test is 5.3% and 2301kg/m^3, respectively.

4.3.2.3 cement-treated base (CTB)

The construction of the CTB layer in the inverted pavement is based on the Vulcan inverted pavement structure. The aggregates used in this round of tests were the same as the last round, which were the Grade D aggregates. 4% (by weight) of ordinary Portland cement (type Ⅰ) was added to the aggregates to build the CTB layer. The materials of CTB were obtained during the construction and tested according to the ASTM D 1633 standard. Based on the test results, its 7-day compressive strength is 4.7 MPa (688 psi) with a density of 2243 kg/m^3 and its moisture content is 6.9%.

4.3.2.4 Asphalt concrete (AC)

The asphalt concrete mixture used in this test is the 411-E type and the asphalt binder belongs to PG 64-22. The detailed mix proportion is shown in Table 4-2. The AC (ASC-HM) used in this study has a theoretical density of 2,553 kg/m^3 and optimum asphalt content of 5.50%.

Table 4-2

Mix proportion of AC

Material	***Size or Grade***	***Percent (%)***
Hard limestone	D rock	47.1
Soft limestone	#10	9.4
Natural sand		23.6
Reclaimed asphalt pavement （RAP）	RAP processed-1/2	15.0
Asphalt binder	PG 64-22	4.9

4.3.2.5 Geogrids

The geogrid used to reinforce the pavement is a type of polypropylene biaxial geogrid. The physical and mechanical parameters are presented in Table 4-3. The actual length and width of geogrids laid on the testing pavement lane were equivalent to the dimensions of the test sections. Figure 4-13 shows the physical appearance of the geogrid.

Table 4-3

Physical and Mechanical properties of geogrids

Properties	***Geogrids***
Aperture size (mm)	25×25
Tensile strength at 2% MD/CMD (kN/m)	14/14
Tensile stiffness at 2% MD/CMD (kN/m)	700/700
Junction efficiency (%)	90%

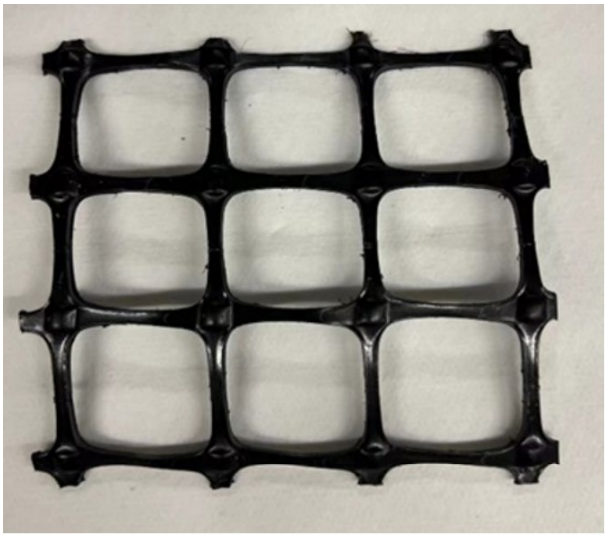

Figure 4-13. Physical appearance of the biaxial geogrid

4.3.3 Layers' Properties

To control the construction quality of the inverted pavement, the nuclear gauge test and DCP test were conducted on each layer of the testing pavement to verify the compaction degree, as shown in Figure 4-14. The same nine points as the 1st round test were chosen to be the testing points. The compaction and moisture content of SG, CTB, UAB, and AC are presented in Table 4-4. To achieve better compaction, each layer was compacted by two or three layer-iterative procedures. Based on the testing results in Table 4-4, the compaction of each layer could meet the requirement.

(a) (b)

Figure 4-14. (a) Nuclear gauge test, (b) Dynamic cone penetration test

Table 4-4

Moisture content and compaction degree of pavement layer

Section	*Compaction (%)*				*Moisture content (%)*		
	SG	*CTB*	*UAB*	*AC*	*SG*	*CTB*	*UAB*
1	92	102	101	92	24.5	4.6	5.5
2	93	92	102	93	22	4.9	5.7
3	91	94	100	94	23	4.5	6.1
4	92	96	98	95	22	4.7	6
5	94	95	99	93	21.5	4.4	6.6
6	90	97	100	94	22.6	4.4	6.4
7	89	99	101	95	23.4	5	5.8
8	96	100	100	93	21.5	4.8	6
9	95	95	100	94	22	4.6	6
Average Value	94.4	96.7	100.1	93.7	22.5	4.7	6
Standard Deviation	2.3	3.2	1.2	1	1.0	0.2	0.3

DCP test could measure the strength the pavement layer after compaction. The relationship between the penetration depth and DCP index of the UAB and SG layers was shown in Figure 4-15.

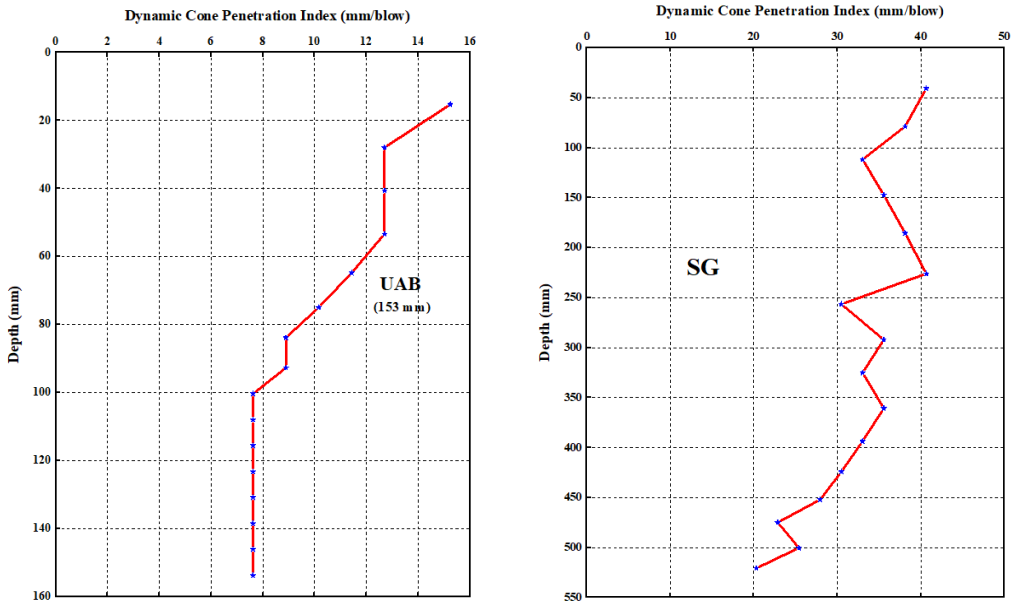

(a) (b)

Figure 4-15. Relationship between penetration depth and DCP index (a) UAB; (b) SG

The penetration depth in UAB layer is between 6 mm and 16 mm, and the penetration depth in SG layer is between 20 mm and 40 mm. In the CTB layer, there is no penetration since the strength of cement mixtures is strong. All the DCP testing points are same as the nuclear gauge test. Based on the penetration depth from DCP test, the predicted CBR distribution can be calculated by Equation (4-1) [6,18]:

$$\mathrm{CBR} = 292/\mathrm{DCPI}^{1.12} \tag{4-1}$$

Where DCPI represents the penetration depth of the DCP test (mm/blow).

Figure 4-16 presents the predicted CBR of the SG, UAB, and CTB layers based on the equation. Based on the calculation results, it can be found that the CBR values of UAB layer are mainly between 10 and 30. The CBR values of SG are mainly between 4 and 10. Due to the high strength of CTB layer, the cone could not penetrate the CTB layer and its CBR value is 100.

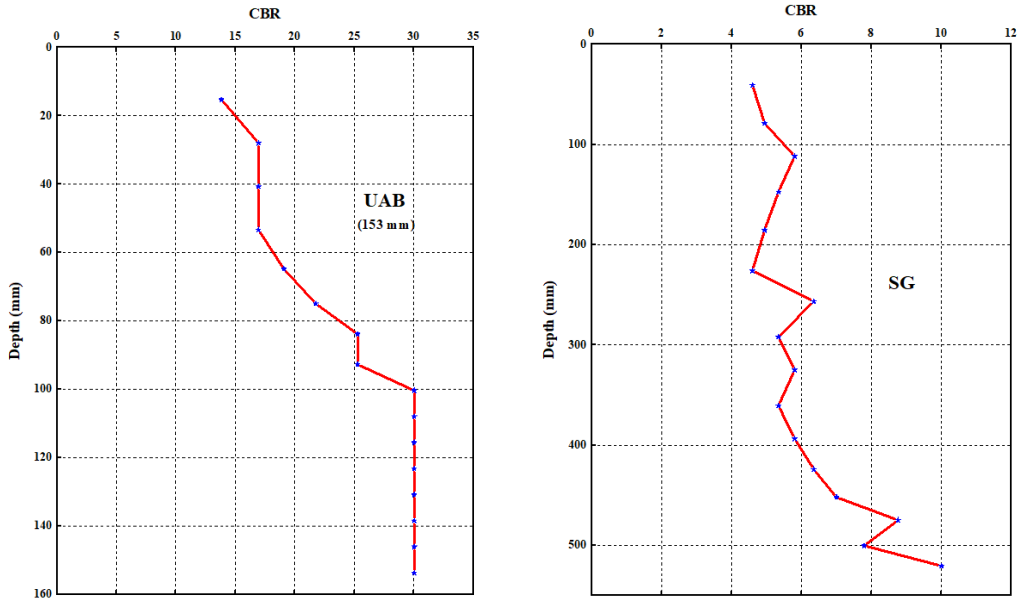

(a) (b)

Figure 4-16. CBR distribution of pavement layers (a) UAB, (b) SG

4.4 Performance evaluation (2nd round)

4.4.1 Surface deformation with loading passes

The loading process of APT is shown in Figure 4-17 (a) and the APT-wheel loading by APT is bi-directional. Figure 4-17 (b) shows the testing points for measuring surface deformation. There are 13 rows and 19 columns in total. After considering the previous test experience and APT equipment capacity, the total loading passes were set as 150 k. The road surface deformation was measured every 10 k loading passes.

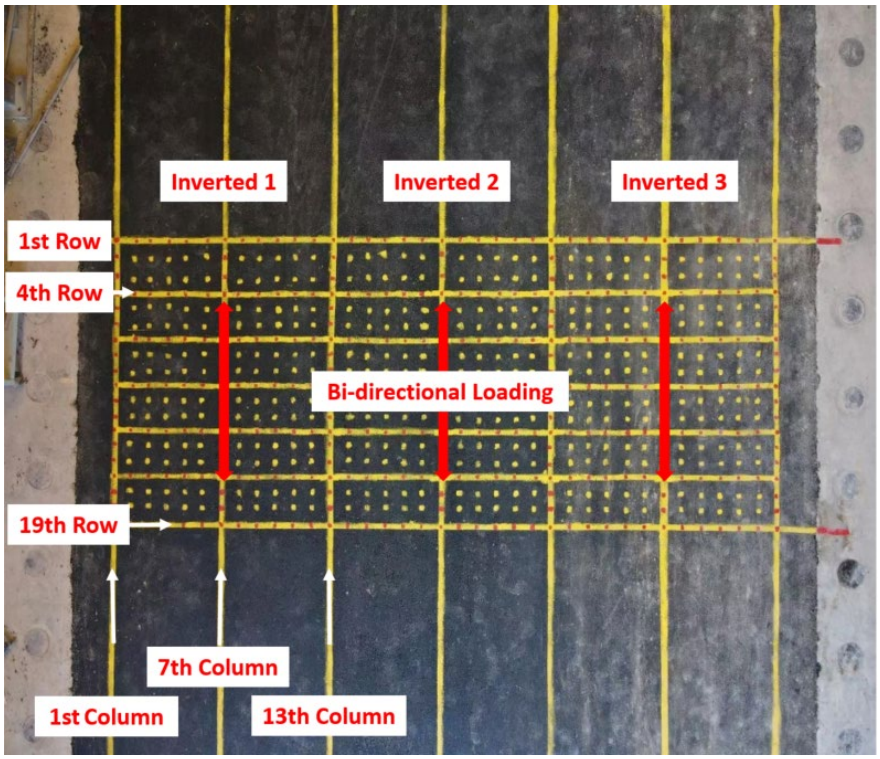

(a)

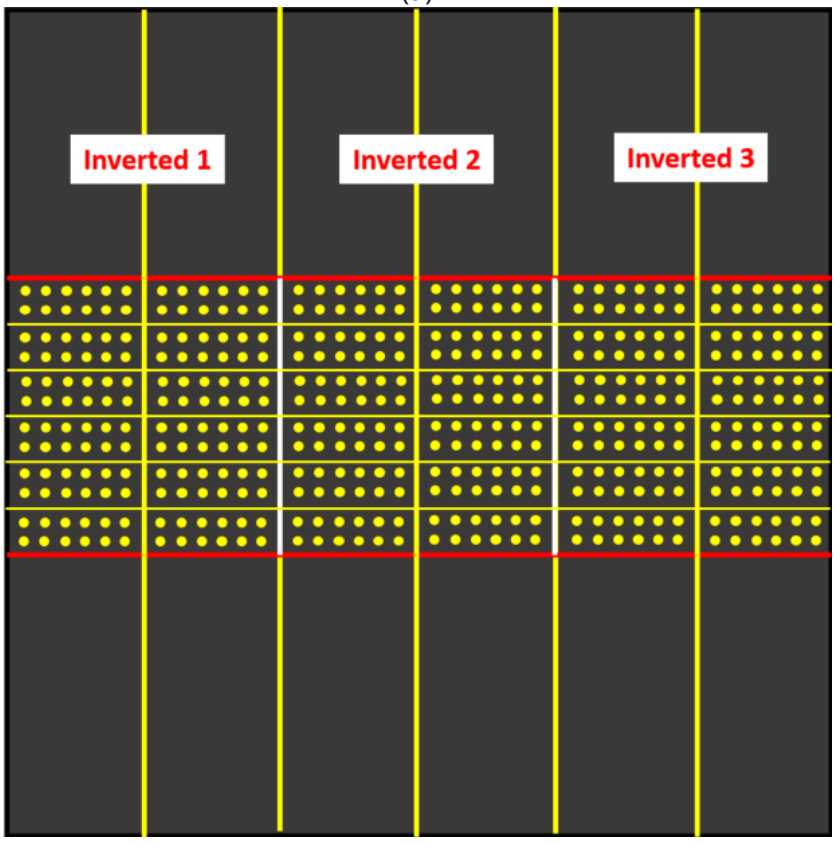

(b)

Figure 4-17. (a) Loading process of APT, (b) Testing points of surface deformation

4.4.2 Transversal surface deformation

The transversal surface deformation of the testing inverted pavement after 150 k of loading passes is shown in Figure 4-18. Each deformation value was the average value of 19 measuring points in the transversal direction. Based on the data in Figure 4-18, the deformation curves of three inverted pavements have the shape of "W" and the main deformation occurred at the wheel-contact areas. The uplift caused by the compression of tire loading was found at the two sides of each testing lane. In the inverted pavement 1, a maximum deformation of 13 mm was found after 150 k loading passes. The maximum deformation of 10 mm was found in the inverted pavement 2 after the APT test. And the inverted pavement 3 has a maximum surface deformation of 6 mm after finishing the whole loading process. According to the FHWA requirement, the rutting depth of flexible pavement over 10 mm could be considered a failure structure[19,20]. Therefore, 10 mm of surface deformation was set as the failure criteria of the testing pavement. Based on the measurement results, the maximum rutting depth of inverted pavement 1 reached 10 mm when the number of loading passes was 70 k. And the maximum rutting depth of inverted pavement 2 reached 10 mm when the number of loading passes was 150 k. However, the maximum rutting depth of the inverted pavement was less than 10 mm after the APT loading process, indicating the best performance of inverted pavement 3. The final rutting performance of the three lanes shows that inverted pavement 3 has the best performance, indicating that the placement of geogrids at the 1/3 thickness from the UAB surface within the UAB layer contributes to the ability of anti-rutting in the inverted pavement. On the contrary, the installment of geogrids at the 2/3 thickness from the UAB surface within the UAB layer could not lead to better rutting performance. Since the UAB layer in the stiffness of inverted pavement has the property of stress dependency, the larger stress is distributed at the upper 1/3 area of UAB layer. The constraint effect of geogrids benefits from larger stress in this area. Under the constraint effect of geogrids, the aggregates in the UAB layer have better interlocking among aggregate particles, contributing to the increase of stiffness in the UAB layer. At the 2/3 area of the UAB layer, the stress is less, pand the geogrids have little effect on controlling the aggregates. In addition, the insert of geogrids would destroy the integrity of the UAB layer, resulting in worse rutting performance compared with the inverted pavement 2 (without geogrids).

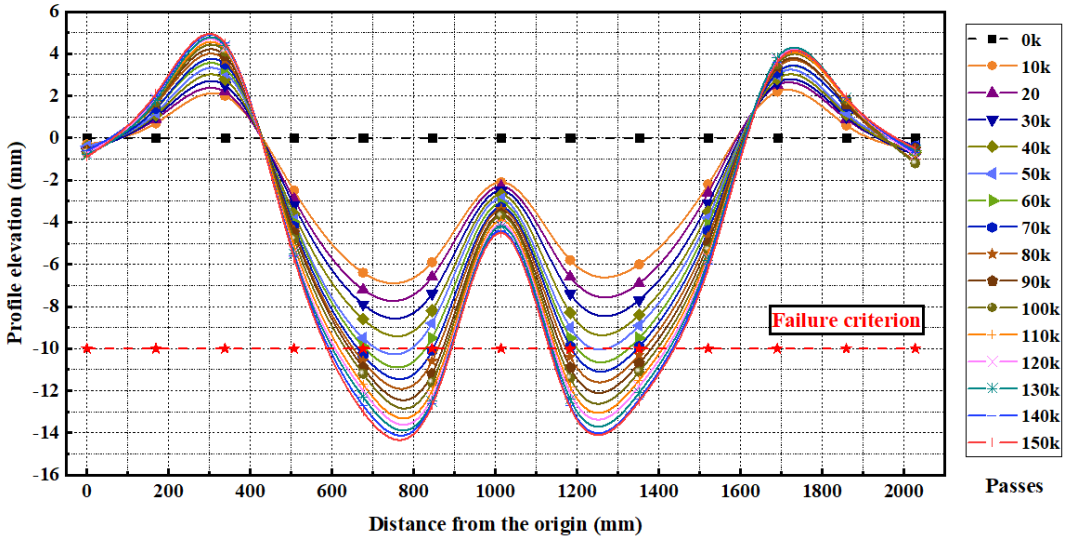

(a)

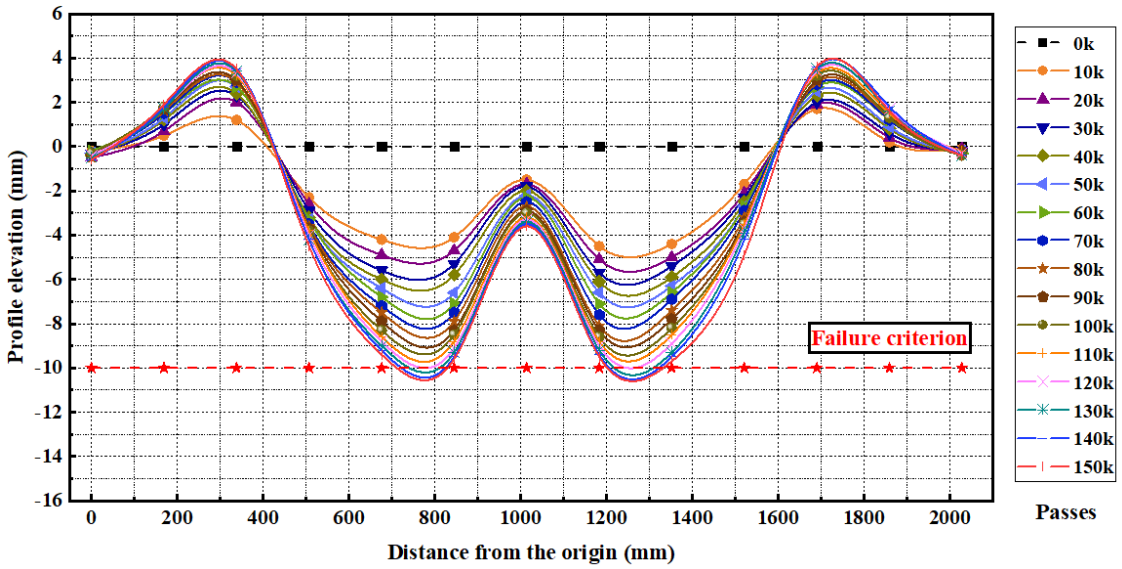

(b)

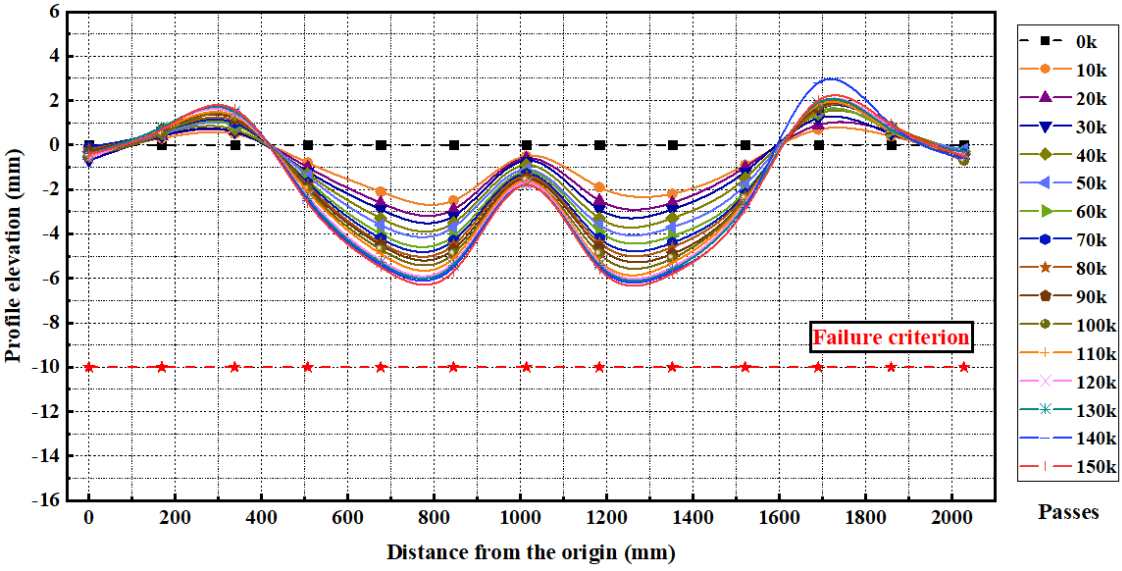

(c)

Figure 4-18. Transversal deformation of testing lanes (a) Inverted pavement 1, (b) Inverted pavement 2, (c) Inverted pavement 3

4.4.3 Deformation contours of inverted pavements

The deformation contours of the testing inverted pavements after 150 k of APT loading passes were presented in Figure 4-19. Based on the data shown in Figure 4-19, the mainly deformed area of the inverted pavement 1 is between 150 mm and 350 mm from the centerline of the lane, as shown in Figure 4-19 (a). The mainly deformed area of the inverted pavement 2 is between 150 mm and 300 mm from the centerline of the lane, as shown in Figure 4-19 (b). In the inverted pavement 3, the mainly deformed area is between 150 mm and 300 mm from the centerline of the lane. In addition, the deformation of the lane boundary is within 1 mm. Thus, it could be concluded that the boundary effect among these three lanes was negligible considering the

measurement error. Each test lane would not influence other lanes, contributing to the confidence of the test results.

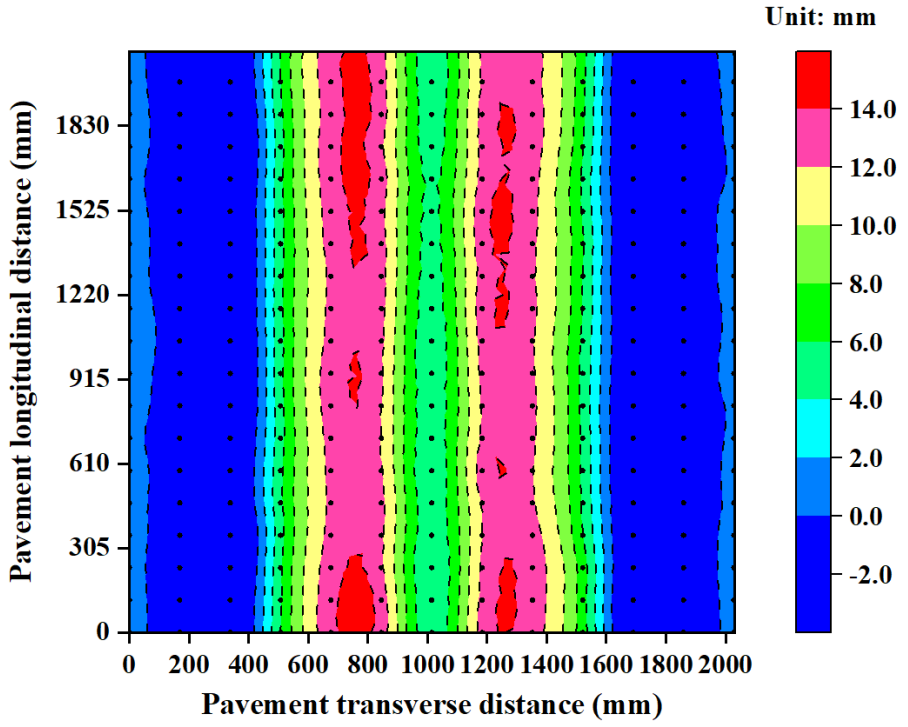

(a)

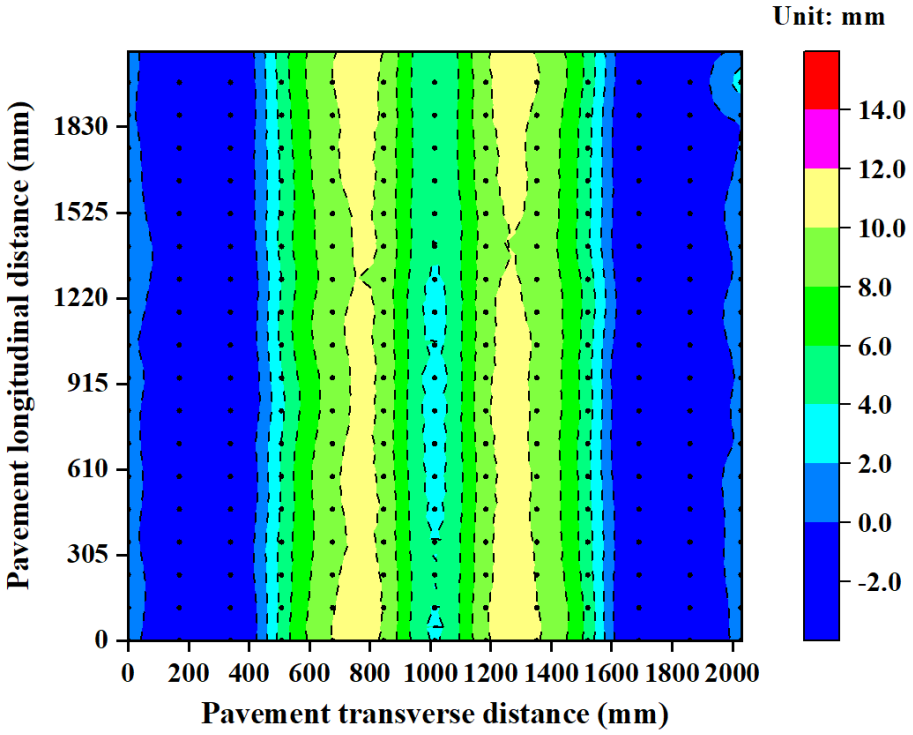

(b)

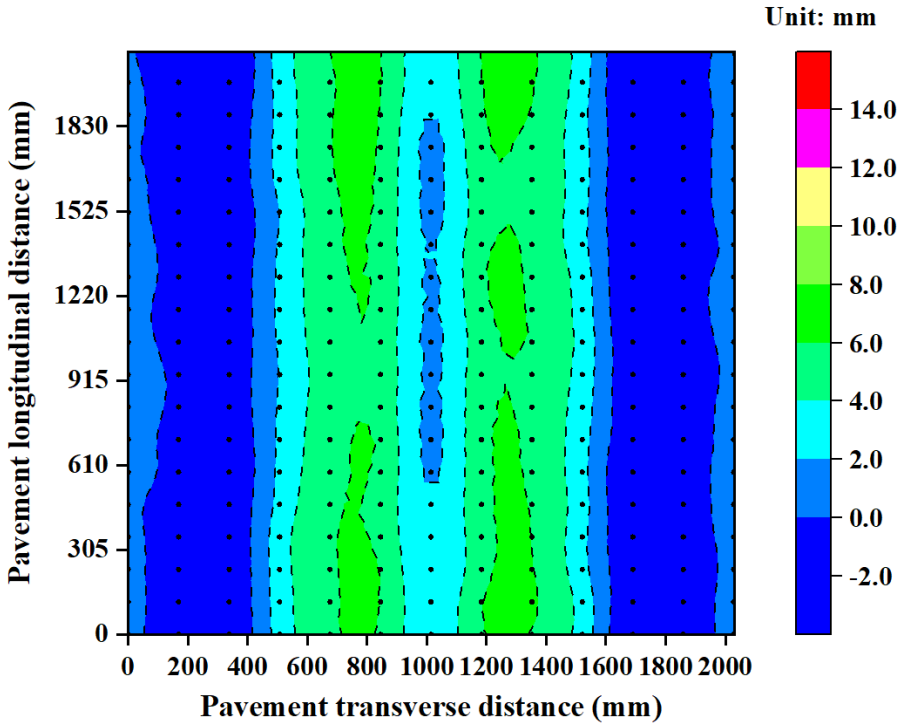

(c)

Figure 4-19. Deformation contours of inverted pavements (a) Inverted pavement 1, (b) Inverted pavement 2, (c) Inverted pavement 3

4.4.4 Development of the maximum surface rutting

Figure 4-20 shows the development of the maximum surface rutting with the loading passes. The average value on the 5th, 6th, 8th, and 9th columns was calculated and the maximum rutting for each lane was obtained. Based on Figure 4-20, the rutting of these three lanes increased a lot after the first 10 k loading passes. In the inverted pavement 1, 6.0 mm of surface deformation occurred after the 1st 10 k loading passes, accounting for 47.1% of the final surface deformation. In the inverted pavement 2, 4.3 mm of deformation occurred after the 10 k loading passes, accounting for 45.0% of the final rutting value. 3.0 mm of rutting happened in the inverted pavement 3, accounting for 38.5% of the final rutting. The above phenomenon was due to the further compaction in the 1st 10 k loading passes. In addition, the E mix of asphalt mixture was used in this test, which contained more fine aggregates, resulting in larger surface deformation compared with the D mix of asphalt mixture. By analyzing the tendency of road surface deformation, it can be found that the maximum rutting of inverted pavements 1, 2, and 3 tend to be stable at 140 k, 130 k and 120 k of loading passes, respectively. In the inverted pavement 3, the deformation is less than 1 mm after 120 k loading passes. The above discussion indicates that the geogrids contribute to the increasing stiffness of the UAB layer in the inverted pavement 3.

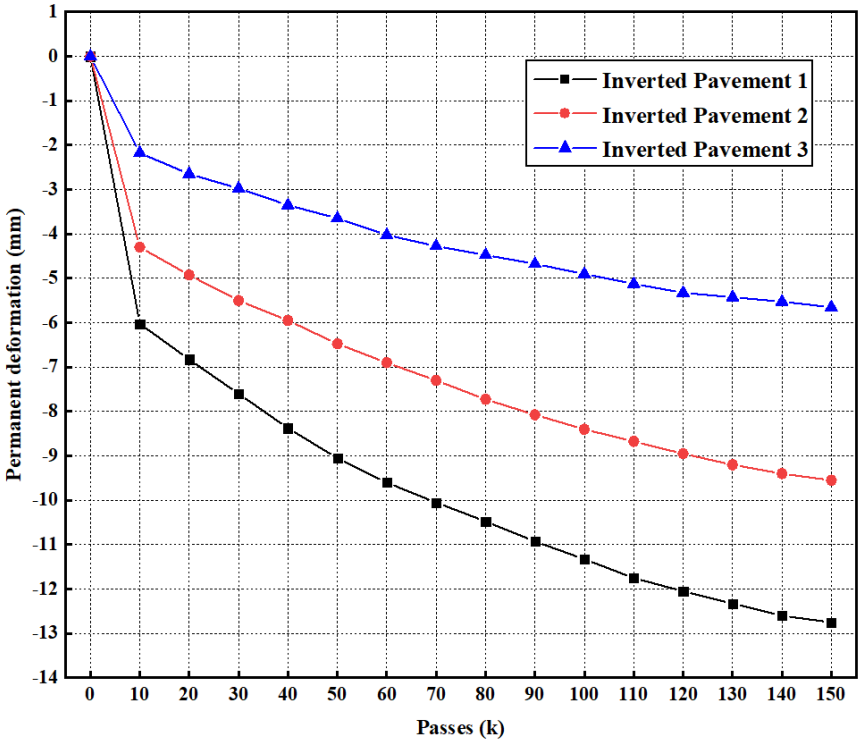

Figure 4-20. Development of the maximum rutting with the loading passes

4.4.5 Effect of geogrids on the performance of inverted pavements

In order to evaluate the reinforcing effect of geogrids in the inverted pavement quantitatively, three evaluation indicators of Rutting Reduction Ratio (RRR), Traffic Benefit Ratio (TBR), and Rate of Deformation (ROD) were used in this study [21–23].

(1) Rutting reduction ratio (RRR)

RRR is defined as the ratio of the rut depth of reinforced aggregate to that of unreinforced aggregate at the same number of load cycles and can be determined by Equation 4-2. The specimen with a lower RRR value usually represents a better rutting resistance performance.

$$\mathrm{RRR} = \frac{d_{reinforced}}{d_{unreinforced}} \tag{4-2}$$

Where $d_{reinforced}$ and $d_{unreinforced}$= rutting depth of reinforced and unreinforced UAB layer at a specific load cycle, respectively. The cumulative rutting depth at the terminal cycle (150 k) was used to calculate RRR.

(2) Traffic benefit ratio (TBR)

TBR is defined as the ratio of the required number of load cycles to reach a certain rut depth in the reinforced aggregate to the required number of load cycles to meet the same rutting depth in the unreinforced UAB layer, as shown in Equation 4-3.

$$\mathrm{TRB} = \frac{N_{reinforced}}{N_{unreinforced}} \tag{4-3}$$

Where $N_{reinforced}$and $N_{unreinforced}$= number of load cycles for reinforced and unreinforced UAB layers, respectively. The threshold of rutting depth used to calculate TBR is selected at which the rutting depth is tented to be stable. TBR is used to reflect the additional load cycles when geogrids are used to reinforce base course materials, and a larger TBR value usually represents a better reinforcement effect.

(3) Rate of deformation (ROD)

Rate of deformation (ROD) is the development rate of permanent deformation and can be calculated by Equation. (4-4). ROD can reflect the rut resistance of reinforced and unreinforced aggregate, and a lower ROD value means a stronger rut resistance for a specimen

$$\mathrm{ROD} = \frac{d_{n+1} - d_n}{t_{n+1} - t_n} \tag{4-4}$$

Where d_n and t_n = permanent deformation of the specimen and the testing time of the nth cycle, respectively.

Table 4-5 shows the final calculation results of evaluation indicators of geogrids in the inverted pavement. Inverted pavement 2 was considered as a benchmark for comparison study. During the calculation of TRB and ROD, the number of loading passes is 150 k. Based on the table, the inverted pavement 3 has the minimum RRR and ROD values but has the maximum TRB value. According to the evaluation indicators, it can be concluded that the placement of geogrid at the upper 1/3 layer of UAB could contribute to the rutting resistance of the inverted pavement structure. However, when the geogrid is installed at the 1/3 lower layer of UAB, the negative of geogrids would be found. Therefore, the inverted pavement 1 has the maximum RRR value and ROD value, and minimum TRB value.

Table 4-5

Evaluation indicators of geogrids in the inverted pavement

Pavement Lane	***Evaluation Indicators***			
	Rutting (mm)	*RRR*	*TRB*	*ROD (10^{-5} mm/s)*
1	*12.75*	*1.34*	*2.40*	*2.36*
2	*9.55*	*1.00*	*1.00*	*1.77*
3	*5.65*	*0.59*	*n/a*	*1.05*

In previous studies, geogrids have been applied to the UAB layer for many years. Jasim et al. [24] investigated the optimum location of geogrids in the pavement base under different loading conditions. The results of this study showed that the geogrids at the upper 1/3 location of UAB had the best performance. Al-Qadi et al. [25] studied the effect of geogrids on the conventional flexible pavement structure. They concluded that the interlayer between the SG and UAB was the optimum position when the UAB had a thin thickness. The upper 1/3 layer was the best installment position when the UAB was thick. Raymond and Ismail [26] investigated the influence of reinforcing positions and reinforcing layers on the rutting resistance of the pavements. The results show that the effect of geogrid depended on both the thickness of UAB and the reinforcing position. When the ratio of reinforcing thickness over UAB thickness was between

0.18 and 0.50, the geogrids played a positive role in the pavement performance. When the ratio was larger than 0.60, the geogrids would have a negative effect on the pavement.

In the APT of this project, the inverted pavement 3 has the best performance regarding rutting depth. And its ratio of reinforcing thickness over UAB thickness is 0.33, which is in the range of 0.18 to 0.50. Therefore, the geogrids improved the rutting resistance of the inverted pavement 3. Nevertheless, the inverted pavement has different structures from the conventional flexible pavement. The UAB layer in the inverted pavement is placed above the rigid CTB layer, rather than the weak SG layer. In addition, the previous studies on geogrid-reinforced pavement did not present the mechanism behind the test results. As a matter of fact, the reinforcement of geogrids in the inverted pavement was affected by the stress distribution within the UAB layer. Due to the stress-dependent property of the UAB layer in the inverted pavement, the geogrids located at positions that are closer to the loading zone will perform better to promote the stiffness increase of the UAB layer. Therefore, the numerical simulations were conducted in the following section.

4.5 Numerical Simulations

4.5.1 Development of constitutive models

To figure out the mechanism of the geogrid-reinforcing inverted pavement, the numerical simulations were conducted by FEM in ABAQUS (software). To simulate the structural responses under the loading accurately, the nonlinear stress-dependent property of the UAB layer was taken into consideration by inserting user-defined materials (UMAT) code in the software. The stress-dependent stiffness property of UAB is the critical point in this study due to its contribution to the structure of an inverted pavement. In previous studies, the resilient modulus calculated by a secant stiffness formulation was used to predict the stiffness of the UAB in numerical simulations. Yoo et al. [27] investigated viscoelastic pavement structures considering the secant stiffness during the model development. Al-Qadi et al. [28] also considered the secant stiffness in a 3-D finite element model. The dynamic responses of flexible pavement under impulsive loading, like a falling weight deflectometer test (FWD), were investigated in the research. However, the process of incremental response in materials is not included in this method. Therefore, a tangent formulation was utilized in this study to model the nonlinear stress-dependent stiffness of UAB. In addition, any arbitrary stress path could be captured in this method.

The resilient modulus of UAB is defined as the ratio of the repeated deviatoric stress to the recoverable part of the axial strain [29]. Among the proposed nonlinear models for the resilient modulus in past studies, the k-θ model or the two-parameter bulk stress model was the most popular model to predict the stiffening and hardening characteristics of UAB [30]. The M_r is calculated by Equation 4-5:

$$M_r = k_1 \theta^{k_2} \tag{4-5}$$

Where M_r represents the resilient modulus, θ represents the bulk stress or sum of principal stresses ($\sigma_1 + \sigma_2 + \sigma_3$), k_1 and k_2 represent the regression constants from the triaxial test.

The softening characteristic of finer aggregate can be calculated by Equation 4-6:

$$M_r = k_3 \sigma_d^{k_4} \tag{4-6}$$

Where σ_d represents deviatoric stress; k_3 and k_4 represent the regression constants.

The above models in Equations 4-6 & 4-7 were widely used in the past due to their easy implementation in FE programs for flexible pavements. However, the shear-stress component for the dimensional change is not considered, which is not suitable for the accurate prediction of thin flexible pavements [31]. Therefore, the octahedral shear-stress term should be added to the model. The stress-dependent behavior of an inverted pavement can be predicted by Uzan's resilient modulus model. This model considers the dilation effect induced by the large principal stress ratio. As shown in Equation 4-8, a fixed-point iteration algorithm is used to implement this model into FEM software.

$$M_r = k\theta^n \tau_{oct}^m \tag{4-7}$$

Where τ_{oct} represents the octahedral shear stress $\left(\sqrt{\frac{1}{3}[(\sigma_1-\sigma_2)^2+(\sigma_2-\sigma_3)^2+(\sigma_3-\sigma_1)^2]}\right)$, and k, n, and m represent the material constants.

However, the fixed-point iteration does not tend to converge when the loads are too large. Thus, a modification was made to predict the resilient modulus based on the strains of the last iteration rather than the previous stresses in the formerly fixed-point iteration algorithm [32]. Equation 4-8 shows the modified model. The nonlinear stress-dependent model in this study was implemented as fixed-point iterations wherein an initial resilient modulus was assumed (fixed) for UAB. A linear analysis of the modulus of UAB was performed using the current value of the resilient modulus. Then, the resulting displacements were used to calculate strains, subsequent stresses, and a new resilient modulus. The process was repeated until the new modulus of the UAB was equal to the value of last iteration, and the process of the analysis from stress to strain could be considered as a strain-based method.

$$M_r = (1+\vartheta)\left[\frac{K}{1+\vartheta}\left(\frac{\vartheta}{1-2\vartheta}+\frac{1}{3}\right)^n\right]^\mu \rho^{\mu n}\gamma^{\mu m} \tag{4-8}$$

Where ϑ represents Poisson's ratio, $\mu = \frac{1}{1-n-m}$, ρ represents the bulk strain or sum of principal strains $= |\varepsilon_1+\varepsilon_2+\varepsilon_3|$, γ represents octahedral shear strain $= \left(\sqrt{\frac{1}{3}[(\sigma_1-\sigma_2)^2+(\sigma_2-\sigma_3)^2+(\sigma_3-\sigma_1)^2]}\right)$, K, n and m represent the material constants.

Before applying the model in software, a lower limit of the octahedral strain in the user subroutine was used to prevent the overflow induced by low computed strains with small loading steps.

4.5.2 Verification of the numerical model

In order to verify the feasibility of the constitutive model in the UMAT program, the GT-PAVE model was utilized to validate the numerical model. The current nonlinear stress-dependent model used in this study was validated by the field data. As shown in Figure 4-21, the detailed pavement design and materials properties for validation were from Tutumluer [33]. The comparison results are presented in Table 4-6. The predicted stress in the vertical direction was just 4.41% higher than the field data. For the predicted deflection at the surface of the AC layer,

only the maximum deflection at the load center was 12.67% higher than the measured data. Therefore, the numerical model can be verified based on the comparison results.

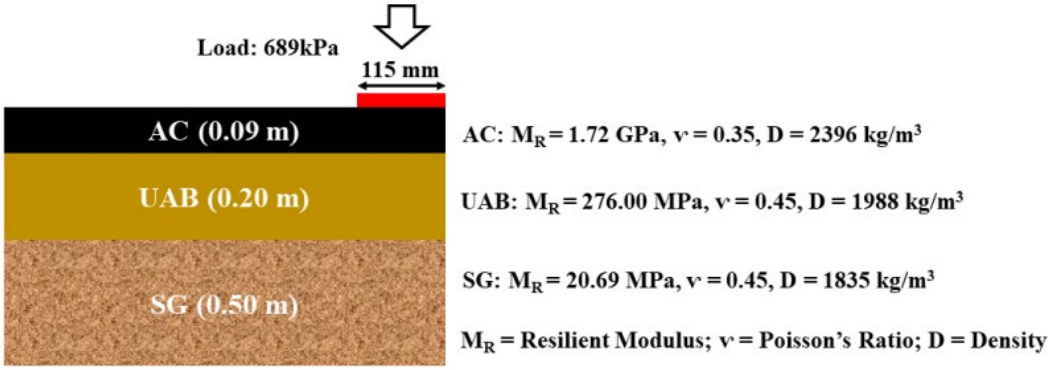

Figure 4-21. GTPAVE conventional pavement structure for model verification

Table 4-6

Comparison of the pavement responses

	Stress (vertical direction) at the top of the SG layer	***Deflection in the AC layer Radial distance (mm)***		
Response	***σ_z (kPa)***	***0***	***254***	***368***
Section 8	*82*	*n/a*	*0.51*	*0.33*
Section 9	*77*	*n/a*	*0.56*	*0.33*
Section 10	*47*	*n/a*	*0.53*	*0.25*
Average(Measured)	*68*	*0.71*	*0.43*	*0.33*
Current model (Prediction)	*71*	*0.80*	*0.44*	*0.34*
Error (%) (Compared to average)	*4.41*	*12.67*	*0.02*	*0.03*

4.5.3 Finite-element model

FEM has been widely used in analyzing the structural response of flexible pavements due to its accurate prediction for construction design. The inverted pavement model in this study consists of a surface AC layer, a UAB layer, a CTB layer, and a subgrade (SG). The conventional pavement model has an AC layer, UAB layer, and SG layer. The schematic design of the pavement structures in the model is shown in Figure 4-22. The left lane pavement is the typical design of an inverted pavement. The middle lane is also an inverted pavement with a different thickness of UAB and CTB for comparison with the left. These two inverted pavement structures were designed to compare the effect of the thickness of the UAB layer and CTB layer. The right lane as the benchmark is a conventional pavement structure used to compare the structural responses to that of the inverted pavements. A quarter of the whole geometry, as shown in Figure 4-23, is modeled to simulate the pavement structure in this study due to the double symmetry of the dimensions of the structures. The length and width of the quarter domain were modeled to be 1.0 m and 1.0 m respectively.

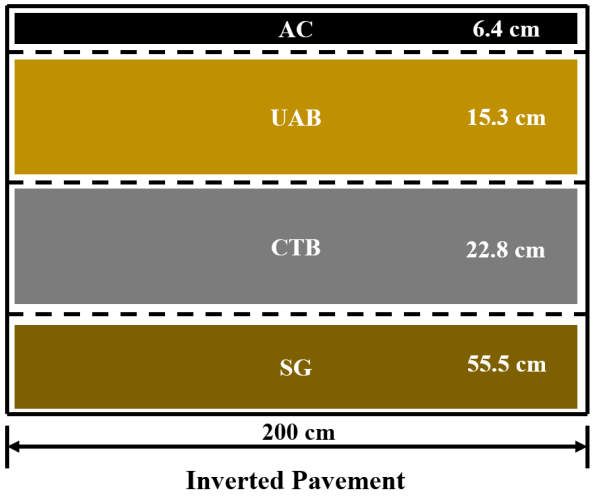

Figure 4-22. Pavement structures in the model

4.5.3.1 Materials properties

The material properties of all the pavement structures in this study for the structural response study are summarized in Table 4-7. These parameters of materials are collected from lab tests and other verified literature [10,34]. The model in this study considered the UAB as a type of elastic material, and its initial elastic modulus of UAB was set at 100 MPa. The modulus of UAB changed with the iteration process in the simulation.

Table 4-7

Materials properties used in the numerical model

Layer	***Thickness (cm)***	***Elastic Modulus (MPa)***	***Poisson's ratio***	***Density (kg/m^3)***
AC	*6.4*	*1700*	*0.35*	*2553*
UAB	*15.3*	*100 (Initial)*	*0.25*	*2301*
CTB	*22.8*	*10000*	*0.25*	*2243*
SG	*55.5*	*50*	*0.45*	*1792*

4.5.3.2 Boundary condition

Proper boundary constraints contribute to the accuracy of the calculation. In this study, the bottom of the SG was constrained, and all types of movements were constrained (ENCASTRE). Roller support was used to simulate the inside vertical surfaces. This support allows translational movement in the vertical direction while restricting the movement in the horizontal plane in respective directions [10,28,35]. The outside vertical surfaces were modeled as free of movement. The top of the model was also free of the boundary. In this model, the interaction between layers was not taken into consideration to simplify the calculation.

4.5.3.3 Loading condition

In previous studies, the equivalent contact area was used to simulate the actual tire contact area as rectangular or circular [36]. The vehicle load in this study adopted the standard single axle with double wheels. And the size of the actual tire marks on the calculation paper is closer to the area of the rectangular area. Thus, as shown in Figure 4-23, the loading area was simplified as a uniformly distributed load on a rectangle area with a length of 10 inches which equaled the actual

contact area. The tire pressure was set at 1.40 MPa based on actual tire pressure on the pavement. The objective of simplifying the load pattern was to improve the calculation efficiency of the model.

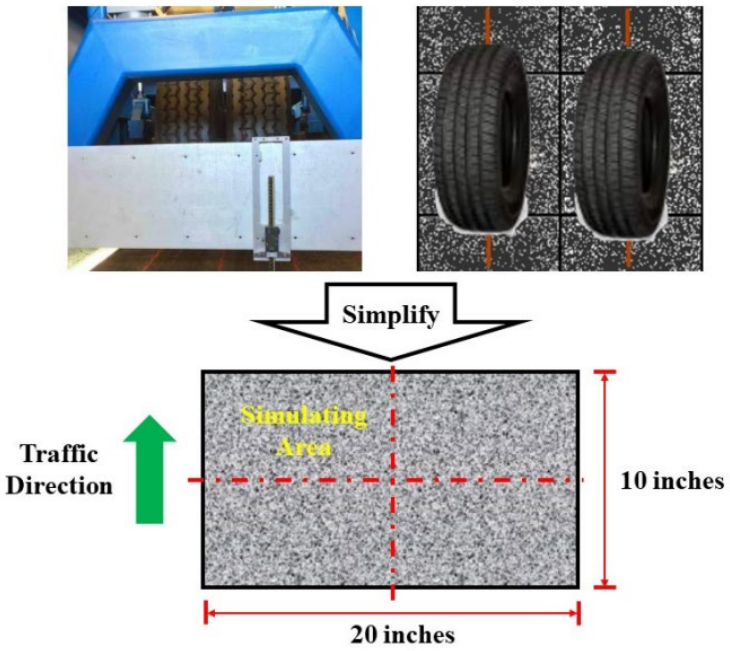

Figure 4-23. Simplified contact area of APT dual wheels

4.5.3.4 Mesh generation

The mesh size contributes to the accuracy of the simulation in FEM [10]. The C3D8 type mesh was applied in this research to minimize the calculation time and improve accuracy. A varying mesh can improve the calculation results. The approximate element size is 0.05, and the deviation factor of curvature control is 0.1. Meanwhile, finer mesh refinement was set for upper layers due to the loading area at the top.

4.5.4 Stiffness distribution of the UAB layer

Figure 4-24 (a) shows the stiffness distribution of the UAB layer in the inverted pavement. The modulus contours within UAB present its stress-dependent property in the inverted pavement structure. Based on the data shown in the figure, the maximum modulus of 373 MPa is located in the area under the loading wheel. However, the unbound aggregates could not experience tensile stress, thus the strain distribution was compared in this study. Figure 4-24 (b) shows the strain distribution of the UAB layer in the transversal direction. The positive value of strains in the figure means the tensile strain. In the upper 1/3 location of UAB, the tensile strain is 6.5×10^{-4}, which is larger than 3.1×10^{-4} in the 1/3 lower location. Therefore, a larger tensile strain was developed in the upper 1/3 layer of UAB, which contributed to the constraint function of geogrids. Therefore, the geogrids improved the rutting resistance of the inverted pavement 1 in the APT test when the geogrids were placed at the upper 1/3 thickness of UAB. However, when the geogrids were placed at the 2/3 thickness of UAB, the geogrids could not take effect due to much less tensile stress. The geogrids could not provide enough constraints for the aggregates and the stiffness of the UAB layer would not increase during the loose condition. In addition, the geogrids with little tension might destroy the integrity of the UAB layer, resulting in worse rutting

performance of inverted pavement 3. Figure 4-25 shows the inverted pavement with the geogrids-reinforcement. It can be found that the geogrids in the inverted pavement 3 were installed at a location with much higher stiffness, and the constraints for the aggregates could benefit from the condition. But the geogrids in the inverted pavement 1 could not work properly.

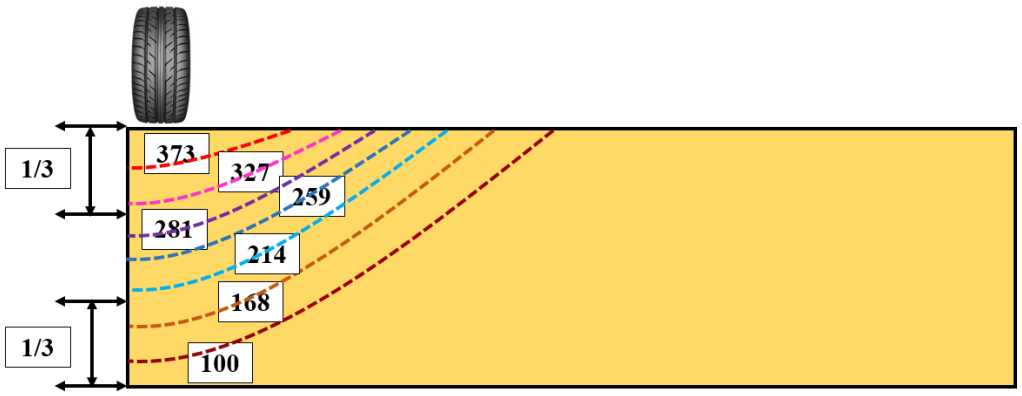

(a)

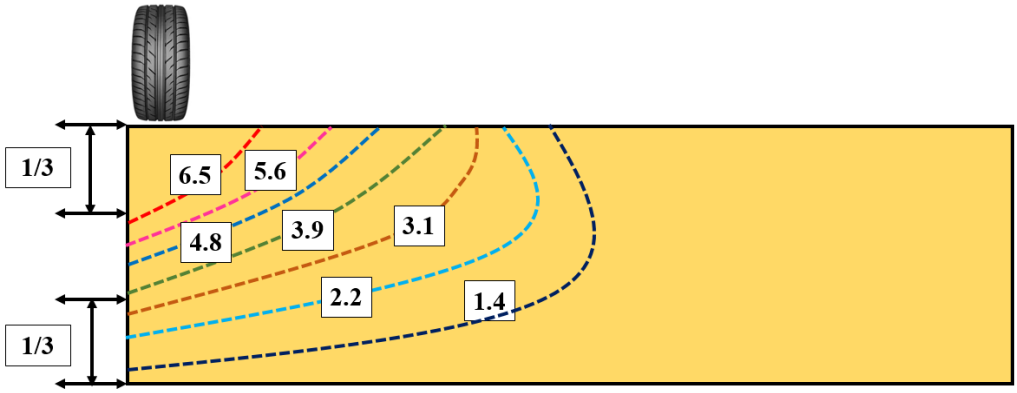

(b)

Figure 4-24. (a) Stiffness (MPa) distribution within the UAB layer, (b) Transversal Stain (E22) ($\times 10^{-4}$) distribution within the UAB layer

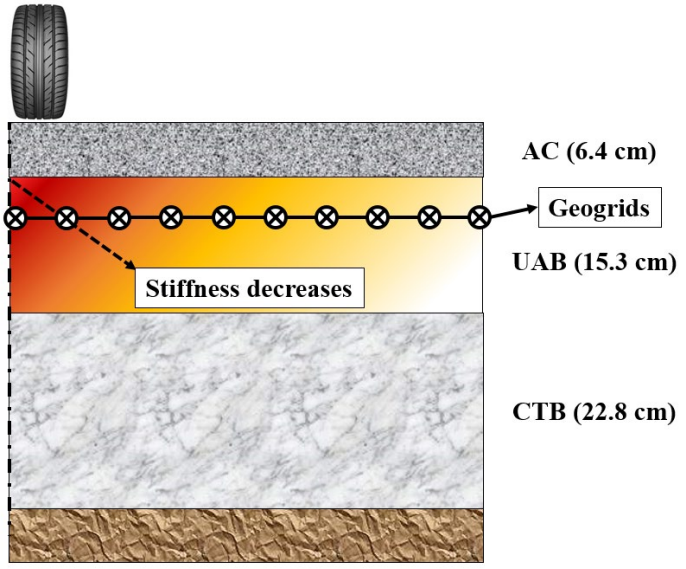

(a)

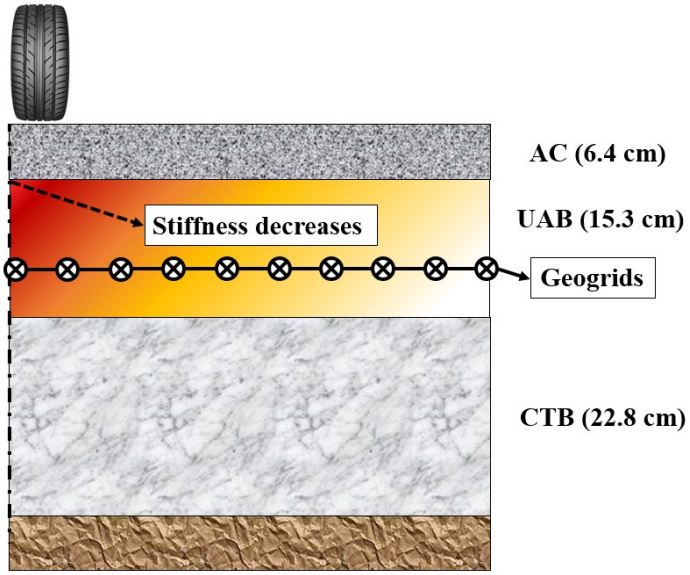

(b)

Figure 4-25. Inverted pavement with the geogrids-reinforcement (a) Inverted pavement 3, (b) Inverted pavement 1

4.5.5 Trench investigation

The testing inverted pavement was trenched from the middle line of the pit to quantify the reinforcement effect of geogrids after the whole APT test, as shown in Figure 4-26. The permanent deformations were measured by a steel tapeline on the field and calibrated by counting pixels of the photo taken with a high-definition camera. The total permanent deformation was the sum of AC, UAB, CTB, and SG permanent deformations, and these four permanent deformations were represented by symbols U_{AC}, U_{UAB}, U_{CTB}, and U_{SG}, respectively. Table 4-26 shows the permanent deformation of each layer in the testing inverted pavements.

Due to the high stiffness of the CTB layer, it is very hard to find deformation of this layer, and its deformation was set as 0 mm. The decrease column in Table 4-8 represents the decreased degree of deformation when the two reinforced lanes were compared with the control section in the middle. The result demonstrates that the overall permanent deformation in inverted pavement 3 showed the best rutting resistance and inverted pavement 1 had the worst performance. Based on the data shown in Table 4-8, it can be found that the deformation of the UAB layer in inverted pavement 3 was 57.1% of inverted pavement 2 (without geogrids). It indicates that geogrids placed at the upper 1/3 layer of the UAB can improve the stiffness of UAB layer. However, the proportion of UAB deformation in the inverted pavement 2 was 4.4% higher than the inverted pavement 2. This phenomenon shows that the geogrids installed at the 2/3 thickness of UAB could not contribute to constraining the aggregates and lead to worse deformation.

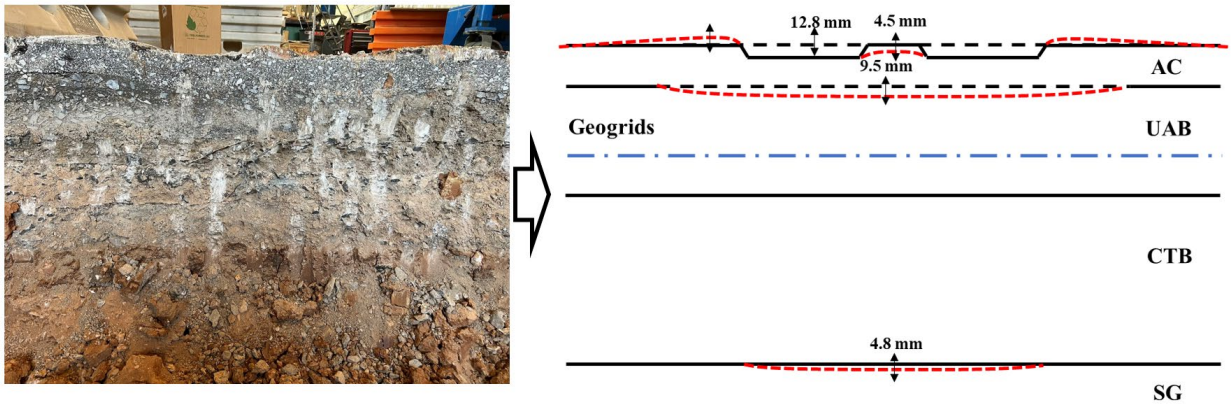

(a)

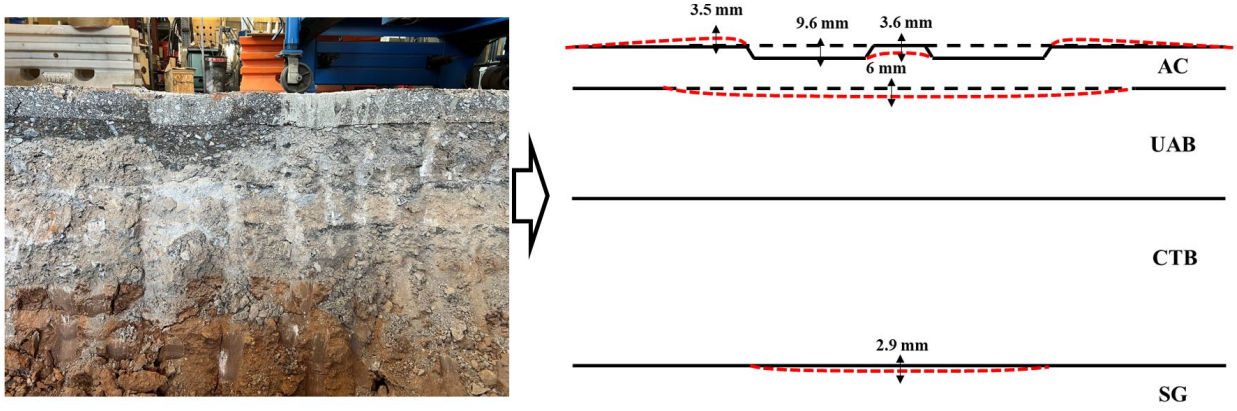

(b)

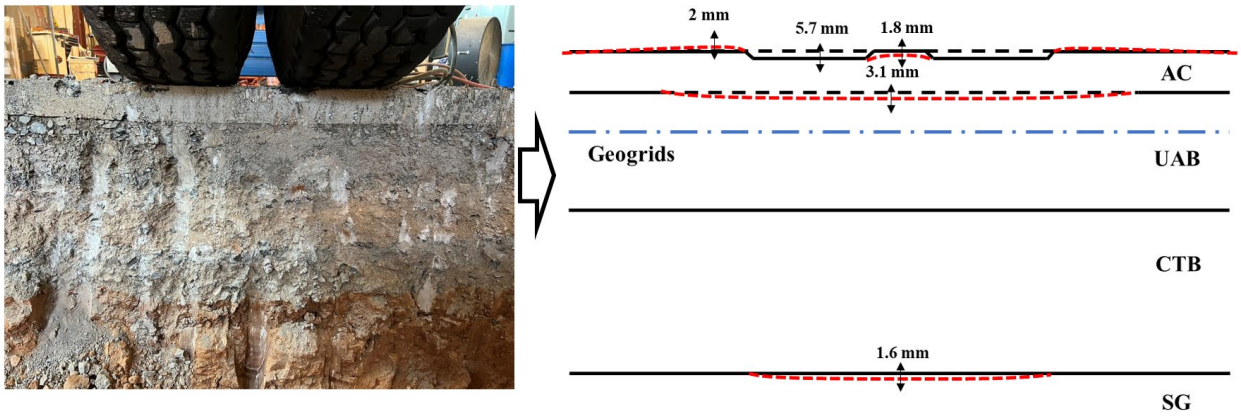

(c)

Figure 4-26. Trench cut in the three lanes (a) Inverted pavement 1, (b) Inverted pavement 2, (3) Inverted pavement 3

Table 4-8

Permanent deformation of each layer in the inverted pavements

Layer (mm)	***Inverted pavement 2***		***Inverted pavement 1***			***Inverted pavement 3***		
	U_L	$\frac{U_L}{U_{total}}$ (%)	U_L	$\frac{U_L}{U_{total}}$ (%)	***Decrease (%)***	U_L	$\frac{U_L}{U_{total}}$ (%)	***Decrease (%)***
AC	*3.6*	*37.5*	*3.3*	*25.8*	*9.2*	*2.6*	*45.6*	*57.8*
UAB	*3.1*	*32.3*	*4.7*	*36.7*	*-51.6*	*1.5*	*26.3*	*57.1*
SG	*2.9*	*30.2*	*4.8*	*37.5*	*-200*	*1.6*	*28.1*	*66.7*
Total	*9.6*	*100*	*12.8*	*100*	*-33.3*	*5.7*	*100*	*55.5*

Chapter 5 Conclusion

In this study, two rounds of the full-scale APT test were used to investigate the performance of the inverted pavement, and a comparison study was conducted between the inverted and conventional pavement structures on the permanent surface deformation. Based on the results and findings from this study, the main conclusions can be drawn as follows.

- Based on the first round of APT test results, the inverted pavement has a comparable performance with the conventional flexible pavement. Therefore, inverted pavement can be considered an alternative to conventional flexible pavement.
- The construction quality plays a significant role in controlling the performance of the inverted pavement. Therefore, the construction processes should be treated carefully.
- Based on the second round of APT test results, the inverted pavement with geogrids could have better rutting resistance. However, the reinforcement of geogrids in the UAB layer depends on the location of the geogrids. When the geogrids were placed at the upper 1/3 layer of UAB, the rutting performance improved a lot. But when the geogrids were placed at the 2/3 thickness of UAB, the inverted pavement had worse rutting.

References

[1] A. Vargas-nordcbeck, The Roles of Accelerated Pavement Testing in Pavement Sustainability, 2016. doi:10.1007/978-3-319-42797-3.

[2] W.J. Steyn, Significant Findings from Full-Scale Accelerated Pavement Testing, 2012. doi:10.17226/22699.

[3] J. Ling, F. Wei, H. Zhao, Y. Tian, B. Han, Z. Chen, Analysis of airfield composite pavement responses using full-scale accelerated pavement testing and finite element method, Constr. Build. Mater. 212 (2019) 596–606. doi:10.1016/j.conbuildmat.2019.03.336.

[4] L.P. Ingrassia, A. Virgili, F. Canestrari, Effect of geocomposite reinforcement on the performance of thin asphalt pavements: Accelerated pavement testing and laboratory analysis, Case Stud. Constr. Mater. 12 (2020) e00342. doi:10.1016/j.cscm.2020.e00342.

[5] M. Fladvad, S. Erlingsson, Permanent deformation modelling of large-size unbound pavement materials tested in a heavy vehicle simulator under different moisture conditions, Road Mater. Pavement Des. (2021). doi:10.1080/14680629.2021.1883464.

[6] B. Han, P. Polaczyk, H. Gong, R. Ma, Y. Ma, F. Wei, B. Huang, Accelerated Pavement Testing to Evaluate the Reinforcement Effect of Geogrids in Flexible Pavements, Transp. Res. Rec. 2674 (2020) 134–145. doi:10.1177/0361198120935120.

[7] D.E. Lewis, D.M. Jared, K. Drive, F. Park, Construction and Performance of Inverted Pavements in Georgia Keith Ledford Pavement Testing Engineer – Pavement Management Branch Georgia Department of Transportation, Transp. Res. Board 91st Annu. Meet. 4214 (2012).

[8] D.D. Cortes, J.C. Santamarina, The LaGrange case history: Inverted pavement system characterisation and preliminary numerical analyses, Int. J. Pavement Eng. 14 (2013) 463–471. doi:10.1080/10298436.2012.742192.

[9] E. Papadopoulos, J.C. Santamarina, Analysis of inverted base pavements with thin-asphalt layers, Int. J. Pavement Eng. 17 (2016) 590–601. doi:10.1080/10298436.2015.1007232.

[10] D.R. Biswal, U. Chandra Sahoo, S. Ranjan Dash, Structural response of an inverted pavement with stabilised base by numerical approach considering isotropic and anisotropic properties of unbound layers, Road Mater. Pavement Des. (2019). doi:10.1080/14680629.2019.1595701.

[11] X. Jiang, M. Zhang, R. Xiao, P. Polaczyk, Y. Bai, B. Huang, An investigation of structural responses of inverted pavements by numerical approaches considering nonlinear stress-dependent properties of unbound aggregate layer, Constr. Build. Mater. 303 (2021) 124505. doi:10.1016/j.conbuildmat.2021.124505.

[12] X. Jiang, J. Gabrielson, B. Huang, Y. Bai, P. Polaczyk, M. Zhang, W. Hu, R. Xiao, Evaluation of inverted pavement by structural condition indicators from falling weight deflectometer, Constr. Build. Mater. 319 (2022) 125991. doi:10.1016/j.conbuildmat.2021.125991.

[13] Tennessee Department of Transportation, Tennessee Department of Transportation Standard Specifications for Road and Bridge, 2015. https://www.tn.gov/content/dam/tn/tdot/construction/old_web_page/TDOT_2015_Spec_Book_FINAL_pdf.pdf.

[14] H. Titi, M. Rasoulian, M. Martinez, B. Becnel, G. Keel, Long-term performance of stone interlayer

pavement, J. Transp. Eng. 129 (2003) 118–126. doi:10.1061/(ASCE)0733-947X(2003)129:2(118).

[15] U.S. Department of Transportation, LOUISIANA EXPERIENCE WITH INVERTED PAVEMENT SYSTEMS LOUISIANA EXPERIENCE WITH FHWA-HIF-19-082, 2017. https://www.fhwa.dot.gov/pavement/sustainability/case_studies/hif19082.pdf.

[16] I.I.A. Qamhia, E. Tutumluer, H. Ozer, H. Shoup, S. Beshears, J. Trepanier, Evaluation of Chemically Stabilized Quarry Byproduct Applications in Base and Subbase Layers through Accelerated Pavement Testing, Transp. Res. Rec. 2673 (2019) 259–270. doi:10.1177/0361198118821099.

[17] B. Han, P. Polaczyk, H. Gong, R. Ma, Y. Ma, F. Wei, B. Huang, Accelerated Pavement Testing to Evaluate the Reinforcement Effect of Geogrids in Flexible Pavements, Transp. Res. Rec. J. Transp. Res. Board. (2020) 036119812093512. doi:10.1177/0361198120935120.

[18] S.L. Webster, Geogrid Reinforced Base Courses for Flexible Pavements for Light Aircraft: Test Section Construction, BehaviorUnderTraffic, Laboratory Tests, and Design Criteria, Tech. Rep. GL-93-6. ASAE Waterw. Exp. Station. Vicksburg, Mississippi, USA. (1992).

[19] T. Grogg, Max；Van, FHWA Computation Procedure for the Pavement Condition Measures, 2018. https://rosap.ntl.bts.gov/view/dot/38327.

[20] Huang，Baoshan;, Zhang，Miaomiao;, H. Gong, Evaluation of Traffic Speed Deflectometer for Collecting Network-Level Pavement Structural Data in Tennessee, 2022. https://rosap.ntl.bts.gov/view/dot/62716.

[21] H. Wu, B. Huang, X. Shu, S. Zhao, Evaluation of geogrid reinforcement effects on unbound granular pavement base courses using loaded wheel tester, Geotext. Geomembranes. 43 (2015) 462–469. doi:10.1016/j.geotexmem.2015.04.014.

[22] P. Selvi, Fatigue and rutting strain analysis on lime stabilized subgrades to develop a pavement design chart, Transp. Geotech. 2 (2015) 86–98. doi:10.1016/j.trgeo.2014.11.001.

[23] G. Wu, F. Chen, X. Pan, M. Xu, X. Zhu, Using the visual intervention influence of pavement markings for rutting mitigation–part I: preliminary experiments and field tests, Int. J. Pavement Eng. 20 (2019) 734–746. doi:10.1080/10298436.2017.1334460.

[24] A.F. Jasim, M.Y. Fattah, I.F. Al-Saadi, A.S. Abbas, Geogrid reinforcement optimal location under different tire contact stress assumptions, Int. J. Pavement Res. Technol. 14 (2021) 357–365. doi:10.1007/s42947-020-0145-6.

[25] I.L. Al-Qadi, S.H. Dessouky, J. Kwon, E. Tutumluer, Geogrid in flexible pavements validated mechanism, Transp. Res. Rec. (2008) 102–109. doi:10.3141/2045-12.

[26] G. Raymond, I. Ismail, The effects of geogrid reinforcement on unbound aggregates, Geotext. Geomembranes. 21 (2003) 355–380. doi:10.1016/S0266-1144(03)00044-X.

[27] P.J. Yoo, I.L. Al-Qadi, M.A. Elseifi, I. Janajreh, Flexible pavement responses to different loading amplitudes considering layer interface condition and lateral shear forces, Int. J. Pavement Eng. 7 (2006) 73–86. doi:10.1080/10298430500516074.

[28] I. Al-Qadi, H. Wang, E. Tutumluer, Dynamic analysis of thin asphalt pavements by using cross-anisotropic stress-dependent properties for granular layer, Transp. Res. Rec. 2154 (2010) 156–163. doi:10.3141/2154-16.

[29] B. Han, J. Ling, X. Shu, W. Song, R.L. Boudreau, W. Hu, B. Huang, Quantifying the effects of geogrid reinforcement in unbound granular base, Geotext. Geomembranes. 47 (2019) 369–376. doi:10.1016/j.geotexmem.2019.01.009.

[30] M.U. Ahmed, A. Rahman, M.R. Islam, R.A. Tarefder, Combined effect of asphalt concrete cross-anisotropy and temperature variation on pavement stress-strain under dynamic loading, Constr. Build. Mater. 93 (2015) 685–694. doi:10.1016/j.conbuildmat.2015.06.031.

[31] D.D. Cortes, H. Shin, J.C. Santamarina, Numerical simulation of inverted pavement systems, J. Transp. Eng. 138 (2012) 1507–1519. doi:10.1061/(ASCE)TE.1943-5436.0000472.

[32] J.M. Duncan, C.L. Monismith, E.L. Wilson, Finite Element Analyses of Pavements, Highw. Res. Board. 38 (1968) 18–33.

[33] E. Tutumluer, D.N. Little, S.H. Kim, Validated Model for Predicting Field Performance of Aggregate Base Courses, in: Transp. Res. Rec., 2003: pp. 41–49. doi:10.3141/1837-05.

[34] D.D. Cortes, J.C. Santamarina, The LaGrange case history: Inverted pavement system characterisation and preliminary numerical analyses, Int. J. Pavement Eng. 14 (2013) 463–471. doi:10.1080/10298436.2012.742192.

[35] U.C. Sahoo, K.S. Reddy, Effect of nonlinearity in granular layer on critical pavement responses of low volume roads, Int. J. Pavement Res. Technol. 3 (2010) 320–325. doi:10.6135/ijprt.org.tw/2010.3(6).320.

[36] B. Saad, H. Mitri, H. Poorooshasb, Three-dimensional dynamic analysis of flexible conventional pavement foundation, J. Transp. Eng. 131 (2005) 460–469. doi:10.1061/(ASCE)0733-947X(2005)131:6(460).